Measurements of a detector prototype with direct SiPM read-out and comparison with simulated data

von

Florian Scheuch

Bachelorarbeit in Physik

vorgelegt der
Fakultät für Mathematik, Informatik und Naturwissenschaften
der Rheinisch-Westfälischen Technischen Hochschule Aachen

August 2010

Erstellt im
III. Physikalischen Institut A
Univ.-Prof. Dr. Thomas Hebbeker

Abstract

This thesis outlines measurements of a detector prototype for muon detection with direct SiPM readout. Special attention has been turned on the reflectors around the scintillator. Therefore cosmic muons have been measured with four different reflectors. Also a thinner scintillator module was measured to determine whether the light yield of smaller modules is sufficient. The data of the different reflectors has been evaluated and is compared to GEANT4 simulations of the setup.

Zusammenfassung

In dieser Bachelorarbeit wurden Detektorprototypen zum Myonnachweis mit direkter SiPM-Auslese vermessen. Ein besonderes Augenmerk wurde dabei auf die verwendeten Reflektoren gelegt, die um den Szintillator gewickelt wurden. Aus diesem Grund wurden Prototypen mit vier verschiedenen Reflektoren vermessen. Ebenfalls wurde ein dünnerer Szintillator vermessen um herauszufinden, ob die geringere entstehende Lichtmenge ausreicht, um den Detektor effizient zu betreiben. Diese Daten wurden ausgewertet und anschließend mit GEANT4-Simulationen des Versuchsaufbaus verglichen.

Contents

List of Figures

List of Tables

1 Introduction

Today particle physics is an important discipline in physics. It is not only used to understand elementary processes but helps us to explore the early universe where these elementary processes are relevant.
For this reason huge particle colliders are designed which are used to be constructed as synchrotrons. At present, the LHC[1] at CERN[2] in Geneva (Switzerland) is the greatest, working collider, currently operated at an energy of 3.5 TeV per beam and a design energy of 7 TeV per beam.

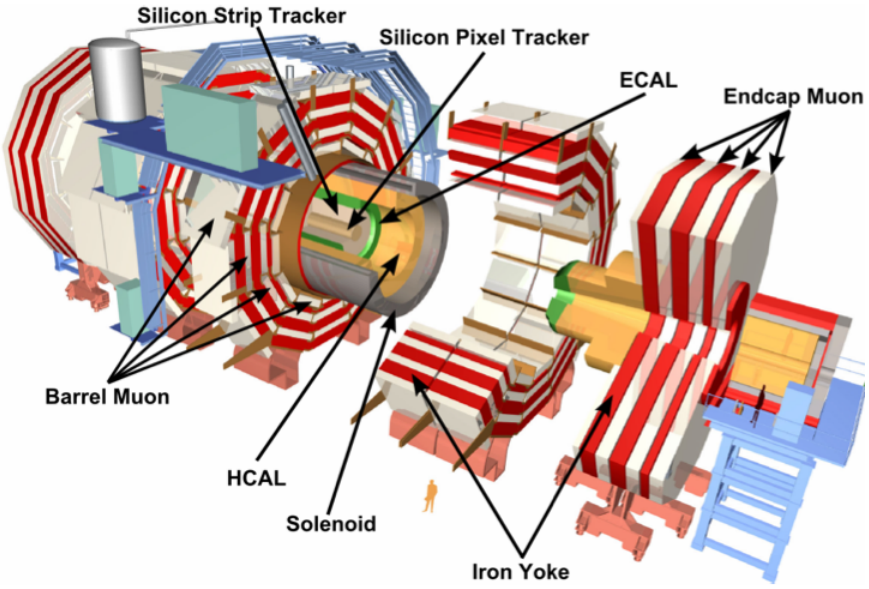

Figure 1.1: The CMS-Detector [6]

[1] Large Hadron Collider
[2] European Organization for Nuclear Research

During the collisions, the four installed detectors (CMS, ATLAS, ALICE, LHCb) measure the produced particles. The RWTH Aachen University is involved in design and operation of the CMS-Detector[3] (Figure 2.2).
Prospectively in 2020 the LHC will be upgraded to SLHC (Super LHC). According to this upgrade the CMS-Detector will be improved, too. Therefore, among others the muon system may be upgraded. At the moment different variations of muon-detection are designed and tested. This is where the topic of the present thesis is located.

[3] Compact Muon Solenoid

2 Muon sources and Muon detection

2.1 Cosmic Muons

Cosmic ray-air showers are a muon source, which is always available. In some experiments

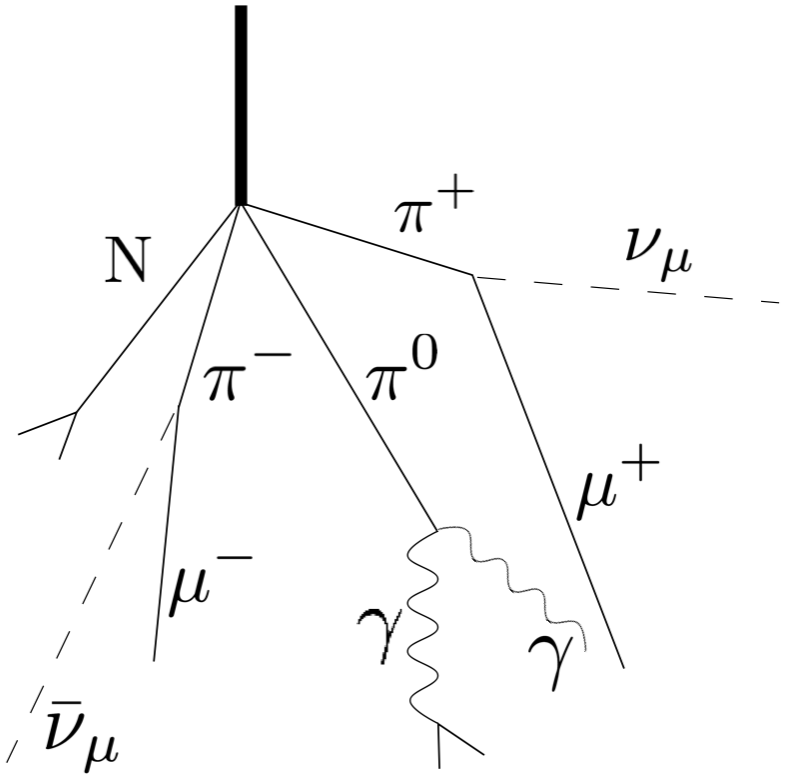

Figure 2.1: Draft of a cosmic ray-air shower (selected events)

cosmic ray-air showers pose a problem, causing background. But cosmic muons can easily be used for basic tests of muon-detector-prototypes, as they are characterized in this bachelor-thesis.

Cosmic-ray air showers develop at a height of approximately 20 km. High-energetic, cosmic particles (e.g. iron or helium) are colliding with atmospheric particles. Thereby, the cosmic particles are split into smaller particles (e.g. nitrogen). Furthermore, pions and photons are created in the collision. The decay of the pion is of interest, because it produces a muon and a muon-anti-neutrino at a rate of 99.99% . Typically, this decay takes place at a height of about 15 km. A distribution of the average number of particles in the cosmic ray-air shower at different altitudes is given in figure 2.2. Since cosmic muons have a very high kinetic energy

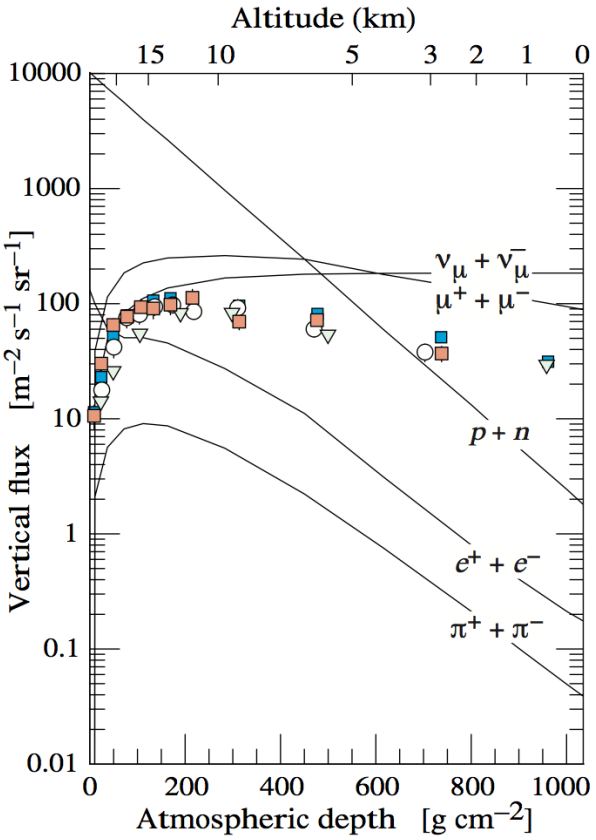

Figure 2.2: Vertical fluxes of cosmic rays in the atmosphere with E > 1 GeV [11]

(velocity $v \sim c$), the mean-lifetime ($\tau 2.2 \cdot 10^{-6}$ s [12]) is stretched according to

$$\tau = \gamma \cdot \tau' = \frac{1}{\sqrt{1-\beta^2}} \cdot \tau'. \tag{2.1}$$

(with τ' as the lifetime in the laboratory system and τ in the muon's rest frame)
So a part of these produced cosmic muons hit the ground and can be detected, before they decay into an anti-electron-neutrino, an electron and a muon-neutrino. The mean-energy of the cosmic muons, which reach the ground, is about 4 GeV [11]. For this energy the parameter γ in equation 4.2 is $\gamma \approx 38$ and the muon's mean-lifetime in the laboratory system is $\tau' = 8,4 \cdot 10^{-5}$ s
For further information see also [11].

2.2 Scintillators

A measurement of particles is only possible when the particles interact with the setup. These interactions are variegated (e.g. ionization, thermal excitation). In general muons are detected by scintillation. The experiments described in this thesis use scintillation for muon-detection, too.
In scintillation (from latin scintillare: flare) a photon or a charged particle ionizes an atom of the medium (the scintillator). This atom releases this energy as light. For a diagram of the scintillation process see fig. 2.3.
The charged particle lifts electrons of the atoms in the scintillator on a higher energy level, often vibrational modes are activated. When the electrons drop back into a lower energy-level, in some transitions fluorescence radiation is emitted. Due to the fact that the electron often does not directly drop back into the valence band, but reaches a vibrational mode, the emitted radiation, caused by the following drop to the valence band, has a lower frequency. For this reason, the scintillator is transparent for the scintillation radiation. Otherwise a detection of scintillation radiation outside the scintillator is impossible, because the emitted light is directly absorbed by the scintillator.
Another important feature of a scintillator is the time that passes from the time of excitation to the time of light emission (fluorescence lifetime). This time span should be less than a few 10 ns. To attain fast readout-rates the fluorescence lifetime has to be in the range of ns.
Scintillators are divided in organic and inorganic scintillators. This distinction is reasonable, because of the very opposing advantages and disadvantages. Inorganic scintillators have a good energy-resolution, but have comparatively a long fluorescence lifetime, are hygroscopic an are expensive compared to the organic scintillators. This is of great interest for huge experiments like the CMS experiment. In contrast organic scintillators have a fast fluorescence

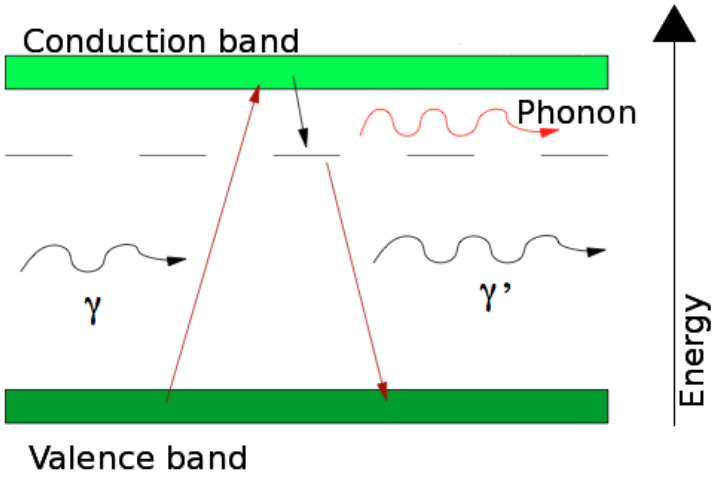

Figure 2.3: Sketch of the scintillation process in the electronic band structure (taken from [20] and modified)

	Anthracene	BGO (Bismuth Germanate)
Light output, Photons/MeV	20000	8000
Decay time, ns	30	300
Maximum luminescence, nm	445	480

Table 2.1: Data of two typical scintillators [8]

lifetime, which can be up to one order of magnitude faster than the fluorescence lifetime of inorganic scintillators. Aside from that, organic scintillators are inexpensive and arbitrary shapeable. The energy-resolution of organic scintillators is inferior to inorganic scintillators. The properties of two typical scintillators (Anthracene and Bismuth Germanate (BGO)) are shown in table 2.1.

2.2.1 Light detection

After the scintillation-light is produced, this light has to be detected in a next step. Nowadays electronic components are used to quantify the light flashes. With these components the light can be detected by much faster rates, which are too fast for the human eye.

Photomultiplier tube (PMT)

On the one hand a photomultiplier consists of a photocathode, which emits a photoelectron, when a photon with a sufficient high Energy (E > work function) hits the cathode. This is called photoelectric effect and was discovered by Heinrich Hertz in 1887 and correctly interpreted by Albert Einstein in 1905 (nobel prize 1921). The emitted photon has a kinetic energy of

$$E_{electron} = E_{photon} - E_0. \tag{2.2}$$

(with the work function E_0)

Several dynodes are placed behind the photocathode (see figure 2.4). These dynodes are on

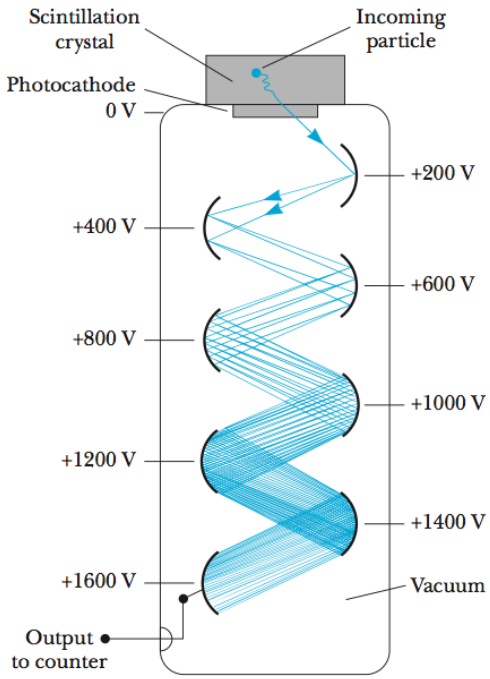

Figure 2.4: Setup of a PMT with a scintillator as light source [21]

different, increasing and equidistant electrical potentials. By use of this potential difference the electron, emitted by the photocathode, is accelerated towards the first dynode. The acceleration enlarges the kinetic energy of the electron. When the electron hits the dynode, secondary electrons are released, which are accelerated towards the next dynode, because it has a higher potential. Step by step more electrons are released on the following dynodes.

An avalanche breakdown occurs. The electrons are collected at the last cathode and cause a charge pulse, which can be measured e.g. an oscilloscope.
A photomultiplier allows high gains (up to 10^7 electrons), which even enables the detection of single photons. But this fact gives rise to the problem that avalanche breakdowns caused by single electrons that are release at the photocathode by thermal noise are triggered although no electron hits the cathode. This effects background noise which has to be cut in the data. Moreover, the photocathode has a quantum efficiency (the probability to release an electron, when a photon hits the cathode) of about 30%. The typical operating voltage of a photomultiplier is in the range of approximately 2 kV [2].

SiPM

Another method of photon detection is the SiPM (Silicon Photomultiplier). The SiPM ist basically a semiconductor diode, connected to a reverse bias voltage.
A diode consists of a semiconductor material (e.g. silicon). The one area of the material is negatively doped, the other one positively. Typically, the doping level has a ratio of $1{:}10^6$. The positive doping causes a lack of electrons in the material (called hole). In contrast, the negative doping causes a surplus of electrons. When the two doped semiconductor materials are connected, the electrons and the holes recombine and an electrical neutral zone occurs in the connection area. The size of this depletion zone is given by [18]

$$d = \sqrt{\frac{2\epsilon\epsilon_0 V_0}{e} \cdot \left(\frac{1}{n_D} + \frac{1}{n_A}\right)}, \tag{2.3}$$

where n_A are n_D the charge carrier densities in the semiconductor and V_0 is the reverse bias voltage.
Accordingly, the size of the depletion zone is proportional to the square root of the reverse bias voltage. When a photon hits the neutral zone of the SiPM, it generates pairs of charge carriers, which are pulled to the poles of the bias voltage. When the charge carriers reach the poles, they can be measured as a voltage pulse. This setup is called avalanche photo diode (APD).
Due to the fact that the APD is operated in the Geiger mode, it is impossible to count the photons, which hit a single APD simultaneously. So it is often of interest to place many APDs at close quarters to measure the number of photons, because if many independent APDs are

placed in close quarters and if the voltage of APDs are parallel merged, the measured voltage gives information about the number of APDs that are hit by a photon. So the measured voltage also gives information about the number of photons, that hit the whole SiPM, when you assume that to a first approximation every APD is hit by one photon only. During a short time of regeneration no more photons can be detected in the APD.
According to the fact that many small semiconductors are placed side by side, not the whole area of the SiPM is sensitive. Some regions of the SiPM are occupied by electronic devices like resistors. These regions are not sensitive to photons. The percentage of the SiPM area that is photon sensitive is called Fill-Factor. This factor depends on the SiPM model.
Furthermore not every photon that hits the sensitive area is detected. The photon detection efficiency

$$\eta_{\text{detection efficiency}} = \eta_{\text{quantum}} \cdot \epsilon \cdot \mathrm{P}_{\text{trigger}} \tag{2.4}$$

(with the quantum efficiency η_{quantum}, the fill factor ϵ and the probability that an incoming photon triggers a breakdown $\mathrm{P}_{\text{trigger}}$ [22]) is higher than the efficiency of the photomultiplier tube and can be up to 75 %. The bias voltage of the SiPM is about 30-70 V which is one order of magnitude lower than the bias voltage of the photomultiplier tube.
Another problem is the temperature dependency of the SiPM's noise and signals. At low temperatures the breakdown voltage is reached with a lower bias voltage than at higher temperatures (see fig. 2.5). Keeping the operating voltage constant causes higher signals and a lower noise rate at low temperature and lower signals and higher noise rates at high temperature (at high temperature the SiPM starts to decline out of the Geiger mode into a proportional mode with standard bias voltage). This characteristic is explainable with the decreasing oscillations of the crystal structure at low temperatures. Therefore the mean free path of the electrons and holes rises so that they are accelerated longer between two collisions in the matter. So the electrons can reach the energy required for the avalanche breakdown much faster [16]. For further information on SiPMs see [7].

2.3 Discriminator

A discriminator is an electronic device that evaluates an input signal and outputs a logical voltage signal when the input voltage exceeds a threshold. When the input signal falls below this threshold again, the logical output signal ends after an arbitrary adjustable time. Normally, the logical signal has an amplitude of -1 V. Two simultaneous signals with differ-

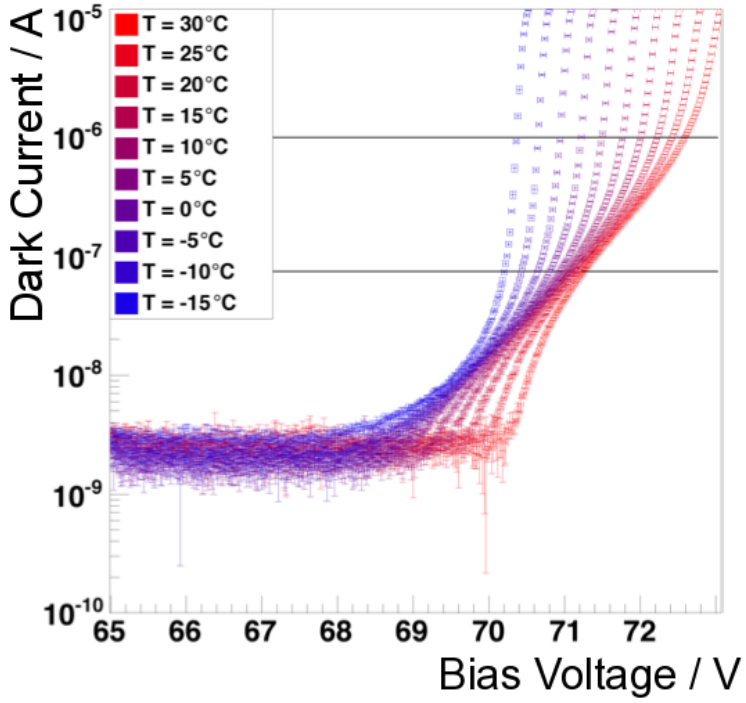

Figure 2.5: Characteristics of a Hamamatsu SiPM Type-50C with 50μm x 50 μm pixels (slightly modified from [16])

ent amplitudes and identical rise time will cause a time shift between output signals (see fig. 2.6(a)). This is a great disadvantage of the basic discriminator.

2.4 Constant Fraction Discriminator

Due to the disadvantage of the basic discriminator used for measurements of coincidences of simultaneous signals with different amplitudes and identical rise time, as they are common in muon detection, one can use constant fraction discriminators. This kind of discriminator divides the input signal into two signals (signals A and B). Signal A is inverted and multiplied by a factor $0.1 < f < 1$. Signal B is delayed by a short time which is smaller than the rise time of the input signal. At the end, both signals are summed (A+B=C) (see 2.6(b)). In the moment, when the signal C reaches a zero value and has a positive slope, the trigger output signal is transmitted. So the trigger signal is not transmitted at a certain voltage threshold, but when

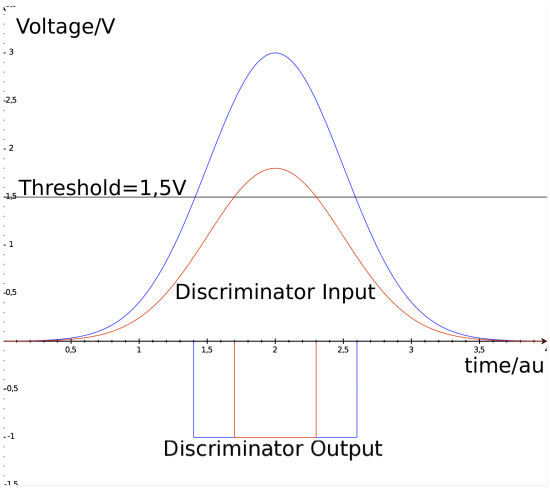

(a) Discriminator in- and output of two simultaneous signals with identical rise time and different amplitudes

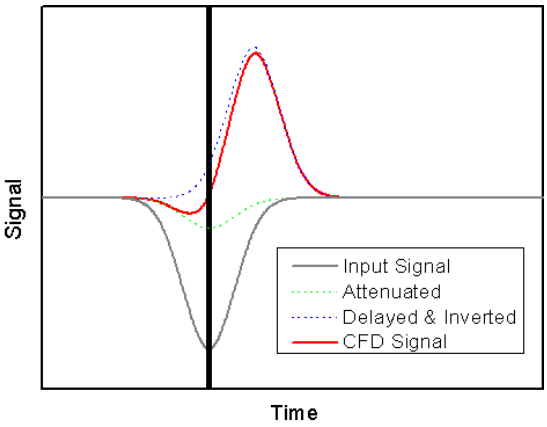

(b) Signal evaluation of a constant fraction discriminator [3]

Figure 2.6: Principles of a threshold and a constant fraction discriminator

the input signal reaches a defined percentage of its total height. The simultaneous signals with different amplitudes and identical rise time will now cause a simultaneous trigger output.

3 Detector setup

3.1 Setup

The whole setup is placed in a metal box, which acts as Faraday cage. Besides, the metal box is light-proof so that no light from outside can affect the muon measurement. The supply voltage for the SiPMs and the amplifiers is lead into the box via a connector plug bridge. Photomultiplier tubes are placed on top and below the box, which can be used to generate trigger signals, so the solid angle can be confined to almost vertical muons (see fig. 3.1).
Due to the fact that the lower PMT and the scintillator on which the SiPMs rest have a sensitive area of 10 x 10 cm^2, are aligned and have a distance of 50 cm to each other, the solid angle of muons that cross the PMT and the scintillator is confined with

$$\Omega = 4 \arctan \frac{w_x \cdot w_y}{2h \cdot \sqrt{4h^2 + w_x^2 + w_y^2}},\ w_x = w_y = 10\text{cm},\ h = \frac{38\text{cm}}{2} \tag{3.1}$$

to 0.26 sr, which is $\frac{0.26}{2\pi} = 4.1$ % of the solid angle (the upper hemisphere) that is visible for the SiPM or the PMT only (With w_x and w_y as the side lengths of the quadratic sensitive areas and h as the half distance between the sensitive areas).
The scintillator is placed on the ground of the black box. The SiPM on the amplifier boards which itself are put inside small metal boxes to avoid electromagnetic rays is directly placed on the top of the scintillator with a bridge holding. The holding can be adjusted such that the SiPM exactly lays on the scintillator. The approximate positions of the SiPMs on the scintillator are shown in figure 3.2.

3.1.1 Scintillator

The scintillator BC-404 by Saint Gobain is used for the detector prototypes. It has a very flat surface, because it is diamond polished which improves the total reflectivity of photons inside the scintillator. The light yield of the BC-404 is 68 % of the anthracene light yield and

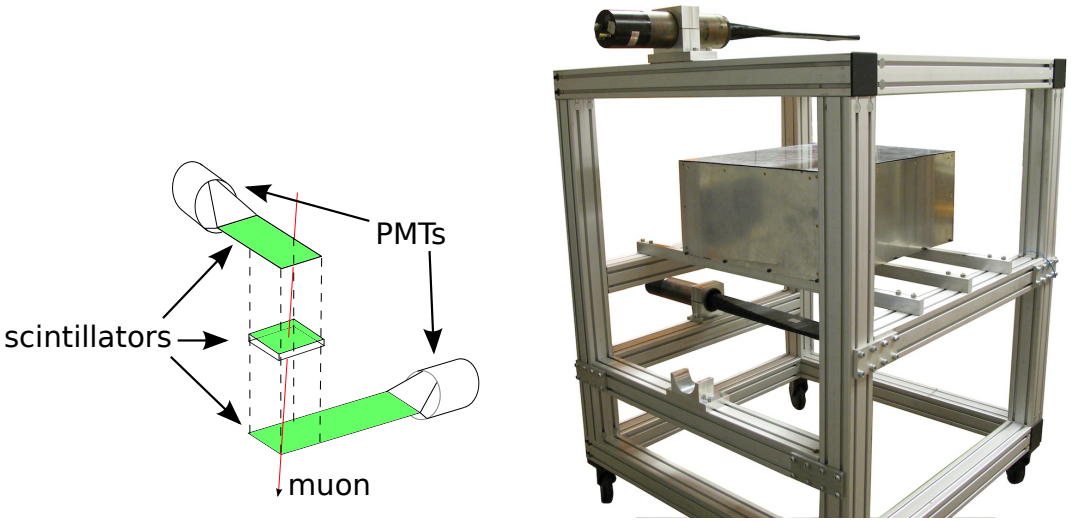

(a) Drawing of the Setup

(b) Picture of the setup

Figure 3.1: Picture and drawing of the setup

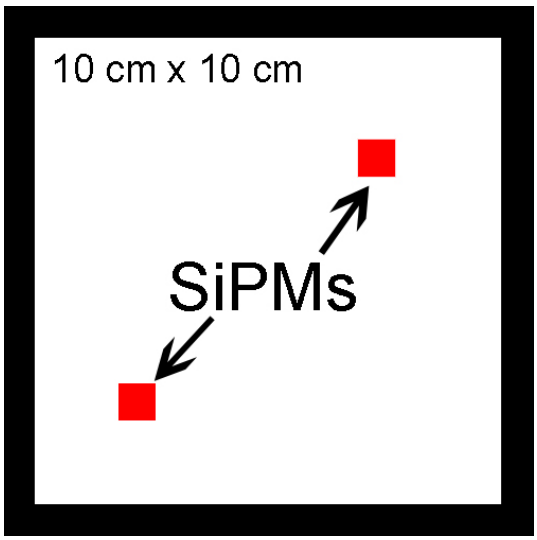

Figure 3.2: SiPM positions (topview, SiPMs are not true to scale)

it has a good light attenuation length of 1.4 m [23]. The decay time of 1.8 ns is very fast.
A diagram of the relative photon incidence depending on the wavelength of the emitted light is given in Figure 3.4(a).

3.1.2 SiPM

The MPPC (multi-pixel photon Counter) S10362-33-100C by Hamamatsu is the SiPM used for the experiments in this thesis. A picture of the used type of SiPM is given in figure 3.3. It is possible to see the single pixels on the SiPM. A list of its features is shown in table 3.1.

Effective Area	3x3 mm^2
Pixel size	100x100 μm^2
Number of Pixels	900
Fill Factor	78.5 %
Gain	$2.4 \cdot 10^6$

Table 3.1: Features of the S10362-33-100C SiPM [13]

The photon detection efficiency depending on the incident photons wavelength is given in figure 3.4(b). This figure shows the data for the S10362-11-100U. This is the same as the used SiPM but with metal case instead of a ceramic case which has no influence on the photon detection efficiency.
A comparison between this dependency and the dependency of the wavelength of the photons emitted by used scintillator shows that the maximum of the emission spectrum corresponds to the maximum of the photon detection efficiency, which is important for precise muon detection.

3.1.3 Amplifier

The amplifier boards designed by Mr. Beißel at RWTH Aachen University (see figure 3.5) are used for the direct amplification of SiPM signals. Each board has a unique ID which is used to identify the boards. The operating voltage is ±5 V. The board has two NiM-outputs: The fast output provides the direct amplified signal without integrating it. This signal is very fast and is used as time signal for triggers. The other output delivers the integrated signal. The signal

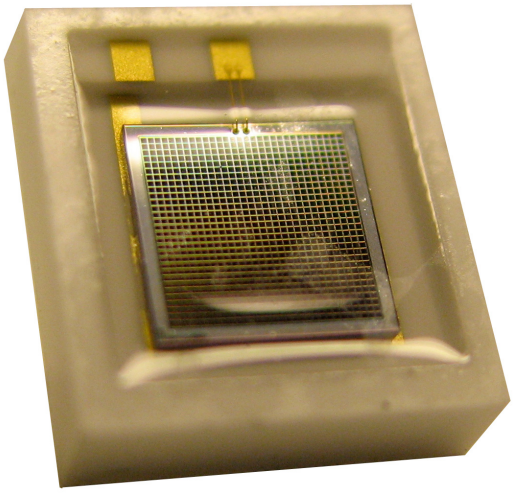

Figure 3.3: Closeup view of a S10362-33-100C SiPM

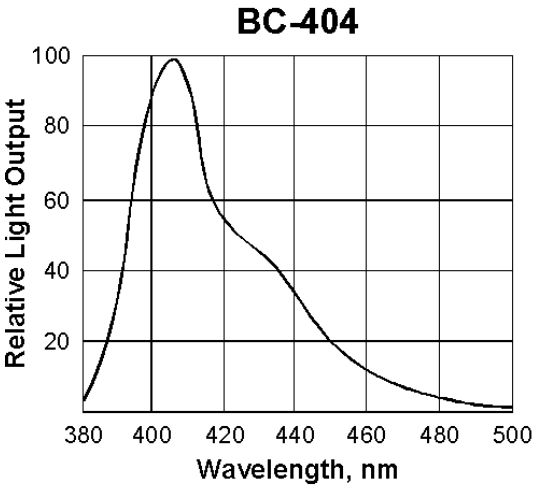

(a) Relative light output of a BC-404 scintillator

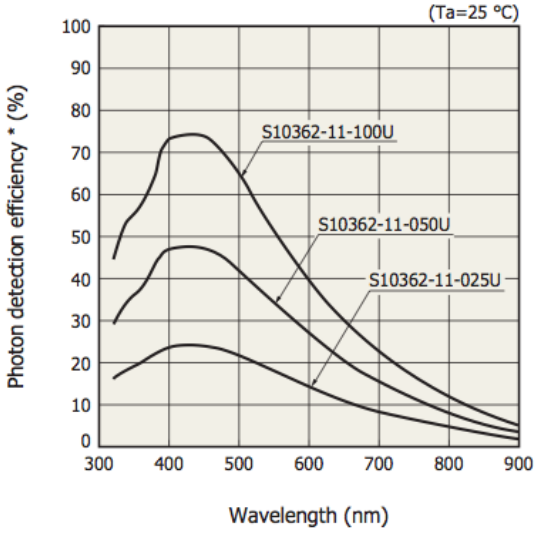

(b) Photon detection efficiencies for three 1 cm x 1 cm SiPMs

Figure 3.4: Dependency of the BC-404 Scintillator an the SiPM on the wavelength [23], [13]

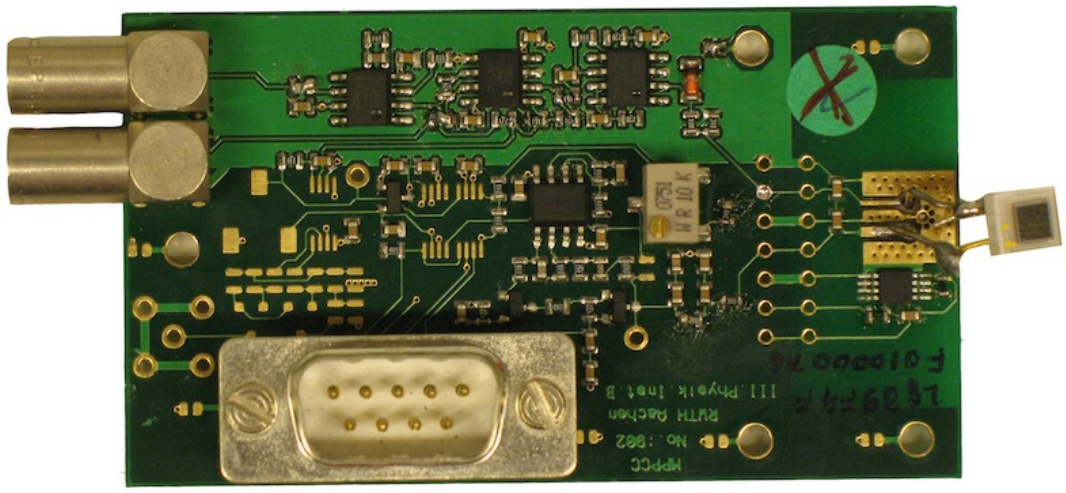

Figure 3.5: Picture of the used amplifier board with a SiPM soldered to the board

at this output was amplified and integrated with a capacitor. So the signal is slower and has a smaller amplitude than the fast output signal. Therefore the integrating output is used for measurements of the charge in the input signal.
The amplifier board maintains the SiPM's supply voltage, too. It is possible to power more than one board with only one voltage source for the supply voltage of the SiPMs, because one can accurately vary the voltage at the SiPM with a trimmer potentiometer on the board. For the circuit diagram of the board see figure 7.1 in the appendix.

3.1.4 Voltage source

SiPM supply voltage

The SiPM supply voltage is provided by the PSI 6150-01 (Elektro-Automatik) which is a linear voltage source. In advantage to a switched-mode power supply, that radiates noise at its switching frequency, the used power supply is a linear controller. This controller is able to produce a fixed voltage of 0-150 V/DC with a stability of < 5 mV and an accuracy of 0,05% at 25°C [10]. So this voltage source is qualified to supply the SiPMs with a precise voltage in the area of 70-75 V.

Amplifiers supply voltage

The operating voltage (±5V) for the amplifier is provided by the EA-PS 2316-050 by Elektro-Automatik which is a linear power supply. The source can provide two different voltages on two outputs in the range of 0-16 V. The signal has a stability of 50 mV. The accuracy is 1 % of the reading plus two digits (at 18°C - 28°C) [9]. This accuracy and stability is good enough for the amplifiers supply, because it needs an operating voltage of 4.5 to 5.5 V.

3.1.5 Pulser

The Pulser is the HP 8082A (Hewlett-Packard) is used for signal production for a test of the amplifiers. This analog pulser has a repetition rate of up to 250 MHz. The pulse signals can almost be arbitrarily shaped within a maximum output amplitude of ±5V and a maximum offset of ±2V. The pulse width can be changed between 2.4 ns and 0.5 ms with a delay of 2 ns to 0.5 ms. The pulses can be given in equidistant intervals by the pulser itself or be tripped by an external logical trigger signal. The output has a 50 Ω impedance.

3.2 Measuring Instruments

3.2.1 Oscilloscope

The signals can be monitored at all stages with the LeCroy WaveJet 354 oscilloscope. This digital oscilloscope has four input channels plus one trigger channel. The four channels can be displayed simultaneously on the 640x480 pixel color TFT-LCD. The vertical sensitivity is 2 mV/division - 2 V/division with an accuracy of 1.5% + 0.5% of full scale [17]. It is possible to change the input impedance to 50 Ω or 1 MΩ. With a rise time of 750 ps and a bandwidth of 500 MHz one can measure small SiPM signals in the order of magnitude of a few 10 mV and a length of a few ns.

3.2.2 Voltmeter

The SiPM voltage is measured with the Multimeter 8842A by Fluke. This desktop device is highly accurate. The accuracy is 0.0015+2 ±(% of Reading + Number of Counts) at the working range of 20 V - 200 V. It enables a measurement at 70 V as it is common during the adjustance

of the SiPMs supply voltage, with an accuracy of 3 mV. The measurement reading is displayed on a digital screen.

3.2.3 QDC

The used QDC (Charge-to-Digital-Converter), model V965 by C.A.E.N. [5] is a VME module with 16 input channels on a 50 Ω impedance. The input charge of each channel is converted to a voltage value by a QAC (Charge to Ampiltude Conversion). These 16 QAC-signals are amplified by factor 1 (Signal A) or 8 (Signal B). These amplified signals are each separately converted by two ADCs (Analog-to-Digital-Converter). For this reason one can get two different resolutions (200 fC LSB (least significant bit) and 25 fC LSB). Now each amount of charge corresponds to a certain QDC channel (with a resolution of $2^{12} = 4096$). Accordingly it is possible to evaluate small signals and greater signals with varying precision. Due to large signals occurring, the 200 fC LSB signal is used in this thesis only.
The signals that have been processed by QDC are transmitted via VME and USB to the PC, through a so called "chained block transfer". This means that the data of 32 events is stored and transmitted to the PC in one block. The PC handles this data and saves it into ROOT-files, which can directly be read out with root.
Plotting the spectra of a channel which had no charge input, one can see a pronounced peak in the number of signals at low counts, which can vary from input channel to input channel. This peak is called pedestal and is caused by an idle current which always flows in the QDC and produces a QDC count. The number of the pedestals QDC count has to be subtracted from the number of the QDC counts of experimentally measured charges, if the channel number is to be converted into a charge value.
The QCD has 4096 channels. Therefore, charges up to $4096 \cdot 200$ pC= 819.2 nC can be measured theoretically. Certainly channels below the pedestal can not be used. Furthermore the QDC collects charge values, which are to high for the QDC, in the overflow, that starts at channel 3840. So the maximum charge that can be measured is less than the theoretical 819.2 nC. The beginning of the overflow at channel 3840 corresponds to the so called 'sliding scale'. The QDC shifts the incoming signals by a random channel number between 0 and 255, evaluates it and shifts it back to improve the differential non-linearity, which describes deviation from the 1 LSP step. A signal that is driven into the overflow is not shifted back so that the overflow has 255 channels.
Addicted to a logical trigger signal that feeds the QDC the time frame for charge measurement

can be arbitrarily regulated.

3.2.4 Temperature sensors

The sensor type DS18B20 by Maxim is used as temperature sensor in the setup. This type of sensor can be read out with a 1-Wire-BUS. Every sensor has its own unique ID, so many of the sensors can be adressed through one data cable. 19 of these sensors are placed side by side on the inner side of the black box. One additional sensor is located on each amplifier board. That way the temperature near the front end electronic can be measured. A list of the temperature sensors features is given in Table 3.2.

Measurement Area	-55 °C to +125°C
±0.5°C Accuracy	-10 °C to +85°C
Readout time	up to 750 ms

Table 3.2: Features of the DS18B20 temperature sensor [19]

4 Measurement

4.1 Characterization of devices

4.1.1 Amplifiers

Because of the SiPMs supply voltage that is provided via the amplifier (75 V, see chap. 3.1.3) it is necessary to conduct a pulser's signal for gain measurements through a capacitor since otherwise the supply voltage would damage the pulser. A measurement of the amplifiers board is presented for the board no. F01000002. For this reason pulses with different amplitudes generated by the pulser (see chapter 3.1.5) with a frequency of 1 kHz are applied through a capacitor (22μF und 44μF) to the place where the SiPM will be placed later. The heights of the output signal of the fast and the integrating output are measured. Input and output signals are measured with an oscilloscope (see chapter 3.2.1). The error on the measured data is estimated to 1% due to the manual reading on the oscilloscope.
The measured data was plotted and a linear regression was fit to the data. The result is shown in figure 4.1.

One can clearly notice that the amplifier's gain depends on the coupling capacitor. So it is not possible to measure the gain with the 75 V supply voltage directly. When the supply voltage is turned off, the gain is not affected though. A measurement without supply voltage and

Measurement	Slope	$\frac{\chi}{\text{ndf}}$
Fast output (22pF)	7.1 ± 0.1	$\frac{10.5}{9}$
Integrating output (22pF)	18.6 ± 0.1	$\frac{11.8}{9}$
Fast output (44pF)	13.6 ± 0.1	$\frac{13.0}{9}$
Integrating output (44pF)	29.9 ± 0.2	$\frac{12.7}{9}$

Table 4.1: Fit parameter of figure 4.1

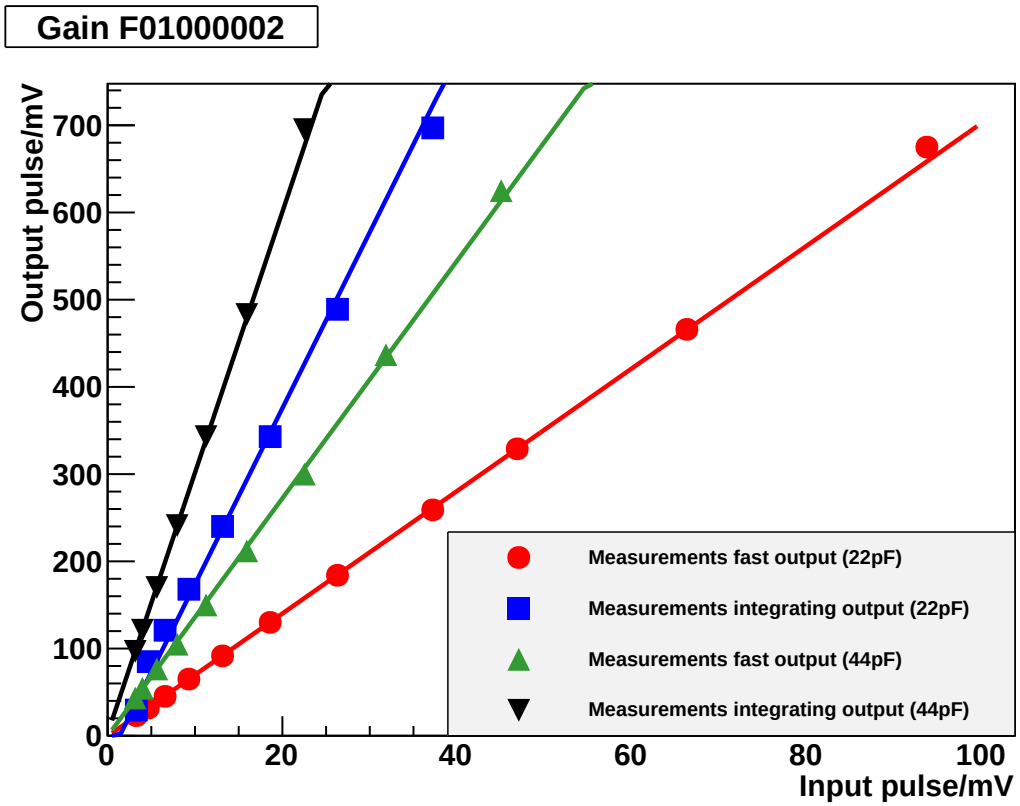

Figure 4.1: The measured gain of the amplifier with a pulser and two different coupling capacitors; see table 4.1 for the fit parameter

without coupling capacitor is procurable with the help of a spectrum analyzer. This device independently transmits signals and measures the answer simultaneously. These measured values are directly converted into a gain value. The advantage of this device is the frequency dependency of the gain that is measured, too. This dependency is especially important for the operation in SLHC where bunch crossing rates of 40 MHz are expected [1]. The measured signals will be very fast and will have pronounced peaks so that high frequency components in a Fourier transformation occur. Therefore the frequency bandwidth from 1 kHz up to 50 MHz and from 1 KHz to 250 MHz (with rougher resolution) was measured. The result is shown in figures 4.2(a) and 4.2(b).

It is obvious that the amplifier's gain decreases with higher frequencies. At high frequencies ($f > 20$ MHz) the decrease of the integrating signal is not linear anymore. This might result

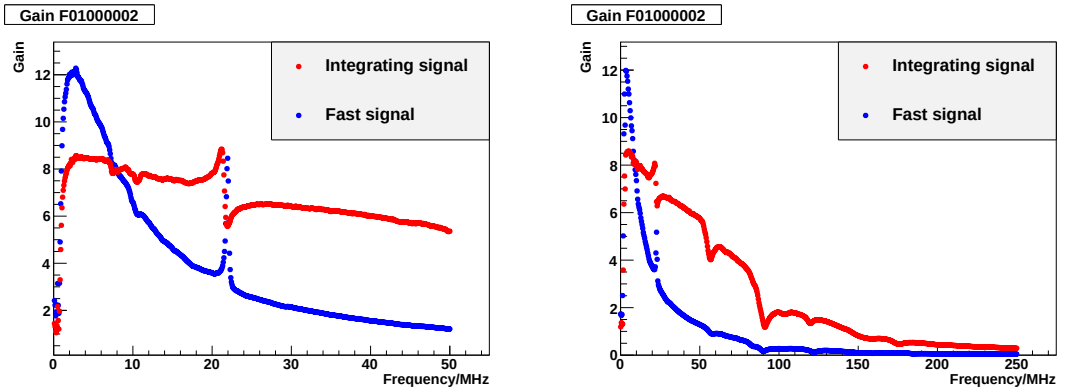

(a) Measurement area: 0-50 MHz

(b) Measurement area: 0-250 MHz

Figure 4.2: Amplifier gain measured with a spectrum analyzer

from resonances on the amplifier board. The decrease of the fast output is not linear in the whole measuring area.
It is indispensable to improve the amplifier electronics to maintain a constant gain over the whole frequency range so that the original shape of the signal is conserved. However these problems are insignificant for the following experiments with cosmic muons, because trigger-rates of a few Hz only will occur.
These measurements were taken with a former version of the amplifier board. The later tests are realized with a new amplifier board with a gain that is 6.5 times lower than the gain of the former boards [F. Beißel, private communication]. This change of the amplifiers became necessary, because first tests with the old boards showed an amplification that drove the output signal into an overflow (see figures 4.3(a) and 4.3(b)), thus no valid QDC data could be taken.

4.1.2 SiPMs

Two SiPMs are used in the setup. In the following they are called SiPM 1 & 2. The data given by Hamamatsu is shown in table 4.2.

A first aim was to measure the the SiPMs dark noise to quantify the emitted charge of a single photon noise that one can interpolate later measurements of the SiPMs charge into a number of photons that hit the SiPM. Therefore it is necessary to see discrete single and multi photon

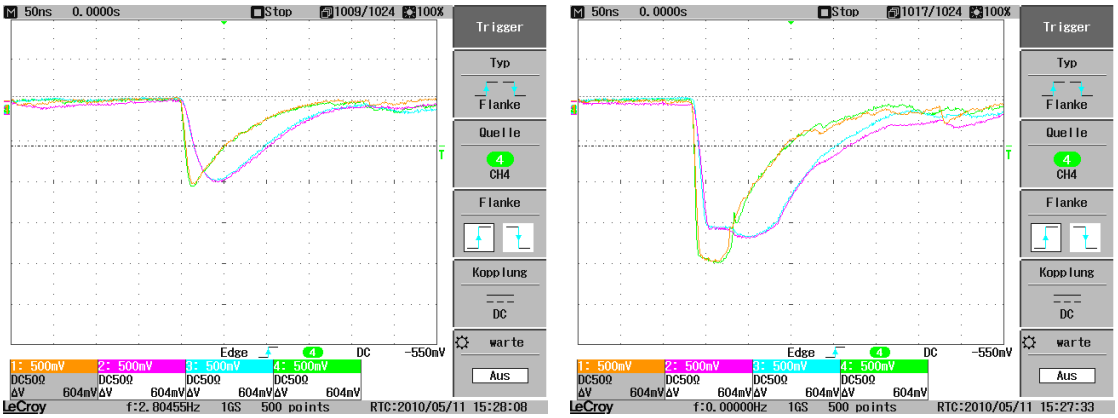

(a) Normal SiPM signals (b) SiPM signals going into overflow

Figure 4.3: Pictures of the SiPM signals of the old amplifier board (green/yellow: fast outputs; blue/violet: integrating outputs; one tick mark = 500 mV x 50 ns)

SiPM	Serial No.	Operating Voltage	Darknoise
1	512	70.91 V	8.4 MhZ at 0.5 photon threshold
2	9J000353	70.91 V	9.3 MhZ at 0.5 photon threshold

Table 4.2: Specifications of the used SiPMs at 25°C

noises at the integrating output on the oscilloscope (see figure 4.4(a) for the noise of a 1x 1 mm^2 SiPM). These discrete photon noises could not be measured at the 3 mm x 3 mm SiPM (see figure 4.4(b)). The number of pixels of the 3 mm x 3 mm SiPM is nine times higher than the number of pixels at the 1 mm x 1 mm SiPM, one can thus expect more noise. More pixels causing noise will result in a higher variability of the noise shape. That is the reason why the noise signal gets blurred with a higher amount if pixels in the SiPM. Because of the missing quantity of the charge of the one photon noise the following analysis has to be limited to a calculation of ratios between different detector setups.

4.2 Measurement of cosmic muons

Cosmic muons where measured with the same type of scintillator (except one for checking the light yield of scintillators with different volume) but different reflectors around the scin-

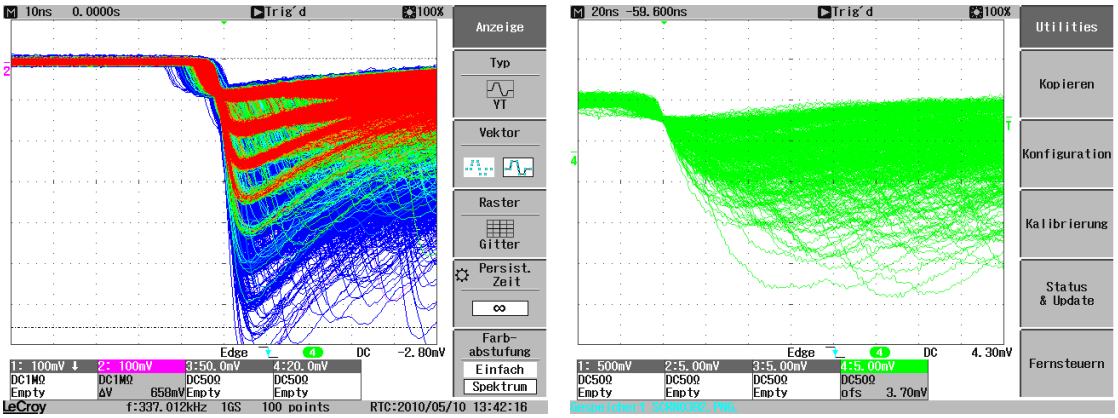

(a) Dark noise of a 1 mm x 1 mm SiPM (one can easily identify single and more photon noise)

(b) Dark noise of a 3 mm x 3 mm SiPM (discrete photon noise can not be detected anymore)

Figure 4.4: Dark noise of a 1 mm x 1 mm and a 3 mm x 3 mm SiPM, the pixel size is $(100x100)\ \mu m^2$

tillator. The arrangements given in table 4.3 have been tested (see also figure 4.5).

Scintillator	Reflector	Reflectivity
(10 x 10 x 0.8) cm^3	Tyvek	90 % [15] [25]
(10 x 10 x 0.8) cm^3	Black felt	~ 0 %
(10 x 10 x 0.8) cm^3	Aluminium foil/bright side	88 % [14]
(10 x 10 x 0.8) cm^3	Aluminium foil/dull side	80 % [14]
(10 x 10 x 0.6) cm^3	Tyvek	90 % [15] [25]

Table 4.3: Measured arrangements of the scintillator (see also figure 4.5)

Due to the fact that the reflector was manually attached to the scintillator without using glue, an air gap between the scintillator and the reflector exists.

4.2.1 Circuit diagram of the setup

The circuit diagram of the setup is given in figure 4.6. The amplifier boards are supplied with ±5 V and 75 V through a serial cable. Also the temperature sensors of the boards are read

Figure 4.5: (10 x 10 x 0.8) cm^3 scintillators wrapped in Tyvek, Aluminium foil/dull side, Black felt (from left to right)

out through one channel of the serial cable (one-wire-bus). The fast output channels of the amplifiers are discriminated with a threshold of -60 mV (discriminators output signal length: 50 ns). This signal is split into two signals of which one is given into one channel of the QDC. The other one is headed into an OR-module that outputs a 200 ns signal with an amplitude of -1 V, if a logical signal is present on at least one of the OR-module's inputs. This output of the OR-module is lead into the trigger input of the QDC. Also the PMT signal is discriminated (threshold: -300 mV; length of output signal: 50 ns) and the output is split. Like for the amplifiers' fast output, the split signal is lead into one QDC channel and in the OR-module. The integrating output of the amplifiers is lead into QDC channels. Therefore if at least one of the SiPMs or the PMT triggers, the QDC records one event within a gate of 200 ns. Several triggers and trigger combinations (e.g. SiPM 1 and PMT triggered) can be applied in the recorded data, because the discriminator signals are recorded, too. It is easy to test if a channel triggered, because the discriminator signal (NIM-pulse) causes a QDC value of ~ 0 (pedestal), if the channel did not trigger and a QDC value in the overflow, if the channel has triggered.
Due to the fact that the PMT has a transition time of 50 ns and the discriminators and the OR-module delay the signal, too, the integrated signals coming from the SiPM outputs had to be delayed with a cable delay by 35 ns and the fast signals by 25 ns that all signals reach the QDC at the same time.
The signals of the 19 temperature sensors inside the box are also read by the PC and the mean of these 19 values is calculated.

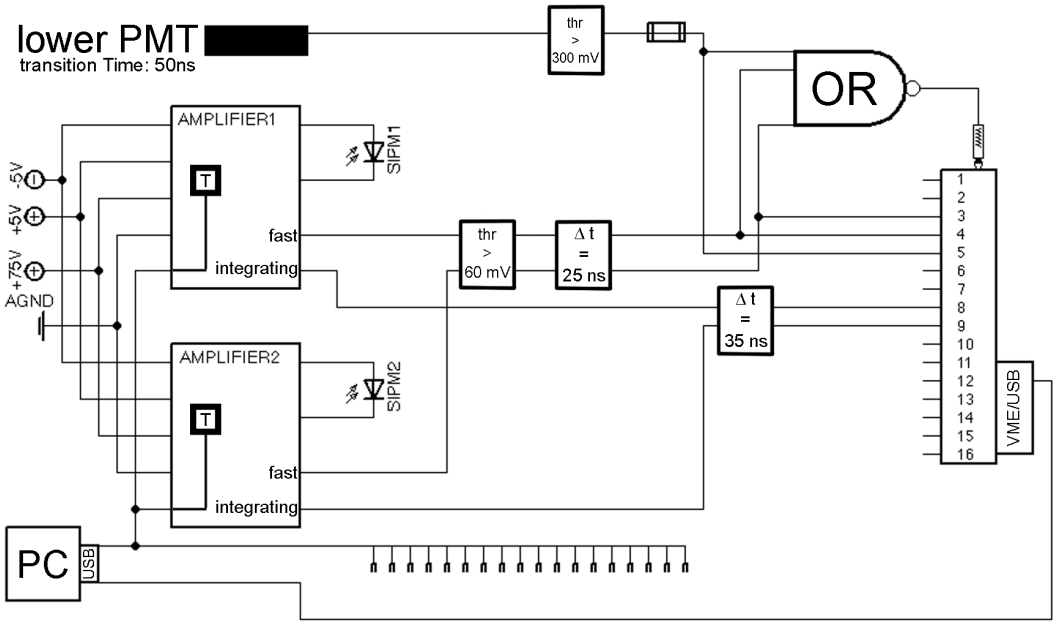

Figure 4.6: Circuit diagram of the setup

4.2.2 Trigger requests

The possibility to determine different triggers subsequently enables the analysis of the data. Therefore different trigger combinations are used, which are explained in the following:

- ▷ No trigger request: The data is not cut. Both the noise and signal are present.
- ▷ SiPM1: It is possible that SiPM1 and SiPM2 triggered or that just SiPM1 triggered. This can also be the case if the noise of SiPM1 is that high (> 60 mV) that it fires a trigger.
- ▷ SiPM2: See SiPM1
- ▷ SiPM1 & SiPM2: The SiPM1 and SiPM2 saw light and triggered. It is mainly the case, when a muon hits the scintillator. The solid angle from which the muon approaches is irrelevant.
- ▷ SiPM1 & $\overline{\text{SiPM2}}$: Here SiPM1 triggers and SiPM2 does not. That means that either it is highly possible that no muon hit the scintillator and that SiPM1 triggered because of its noise, or a muon hit the scintillator and the signal of SiPM2 was too low to exceed the

trigger threshold.

- ▷ $\overline{\text{SiPM1}}$ & SiPM2: See SiPM1 & $\overline{\text{SiPM2}}$.
- ▷ $\overline{\text{SiPM1}}$ & $\overline{\text{SiPM2}}$: Just the PMT triggered. This data represents the noise of SiPM1 and SiPM2.
- ▷ PMT & SiPM1 & SiPM2: A muon crossed the PMT and the scintillator. Due to a gate width of 200 ns (event length) it is very likely that the muon at the PMT is identical to the muon an the scintillator though this trigger request can be satisfied by two different muons although it is very unlikely ($f_{2\mu} = 2 \cdot t_{\text{gate}} \cdot A_{\text{detector}} \cdot \Phi_\mu \sim (10^6\text{s})^{-1}$) with Φ_μ muon flux). This means that these events are due to almost vertical muons.

4.2.3 Temperature dependency

The SiPMs react strongly to temperature variations as described in section 2.2.1. This effect was also found in the measurements, because the temperature in the laboratory varied between 25°C and 30°C during the measurements. The examination of the temperature profiles shows an extreme temperature variation (see figure 4.7) caused by the change of day and night. Remarkably the temperatures on the amplifier boards behave like the temperature in the blackbox. They are only shifted by a temperature difference of approximately 2°C. So it is unimportant on which temperatures the cut is set, as long as the temperature difference is included in the cut.
According to the manufacturer the supply voltage needed by the SiPM changes by 56 mV/°C [13]. Due to the fact that the supply voltage was adjusted only once and was not changes during the measurements, the data is cut to certain temperature ranges. This means that when the cuts are applied only the events are evaluated that are in this temperature range. Table 4.4 shows the used temperature cuts for the different measurements.
The measurement of the 0.6 cm thick scintillator could not be confined to the temperature range of 26°C-28°C, because the temperature in the laboratory was always higher than 28°C during this measurement. This has to be considered in later comparisons of the measurements.

Scintillator	Reflector	T Range/°C	Date (in 2010)/ Time	
			Start	End
(10 x 10 x 0.8) cm^3	Tyvek	26-28	06/22 18:42h	06/28 10:24h
(10 x 10 x 0.8) cm^3	Black felt	26-28	07/02 11:37h	07/05 12:06h
(10 x 10 x 0.8) cm^3	Al-foil (bright side)	26-28	07/06 09:29h	07/08 13:50h
(10 x 10 x 0.8) cm^3	Al-foil (dull side)	26-28	07/08 14:28h	07/11 04:27h
(10 x 10 x 0.6) cm^3	Tyvek	28-30	07/12 14:17h	07/14 13:06h

Table 4.4: Temperature cuts on the data

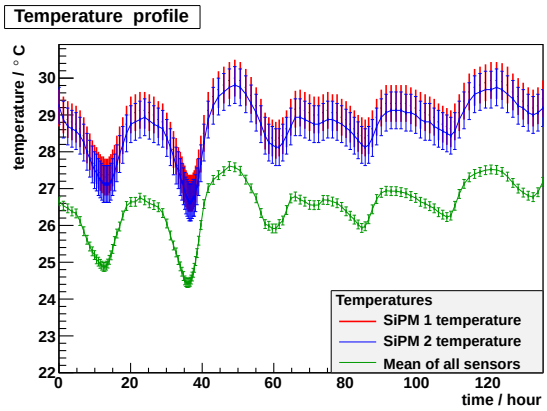

Figure 4.7: temperature profile of the measurement with Tyvek (0.8 cm scintillator thickness)

4.2.4 Measurements

Tyvek (0.8 cm scintillator thickness)

The counting rates of the single SiPMs are strongly varying (figure 4.8(a)) which is caused by the temperature change. Especially the trigger rate is very high at cold temperatures, caused by high noise signals that exceed the discriminator threshold. Interestingly the combination of the trigger requests for SiPM1 and SiPM2 shows an almost constant event rate which is only slightly influenced by the temperature at 3 s^{-1}. The PMT shows no temperature dependency at a constant rate of 4.5 s^{-1}.
The event rates of the trigger requests 'SiPM1 & SiPM2 & PMT', 'SiPM1 & PMT' and 'SiPM2 & PMT' are almost the same (0.11 s^{-1}). So if one SiPM and the PMT saw a muon, the other SiPM saw the muon is the great majority of events, too.

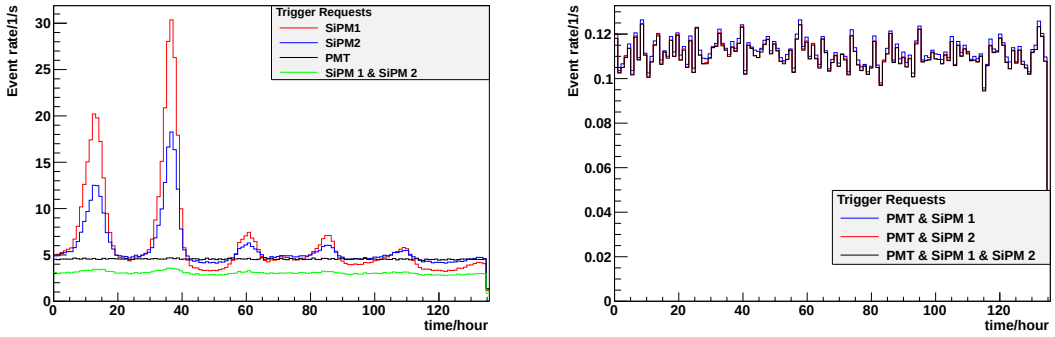

(a) Trigger rates for single detectors

(b) Trigger rates for vertical muons

Figure 4.8: Trigger rates of the measurement with Tyvek (0.8 cm scintillator thickness)

The discussed temperature cuts (section 4.2.3) are applied on all presented SiPM spectra and the pedestal is subtracted. The spectra (figures 4.9(a) and 4.9(b)) without trigger request show both noise and signal. Despite the reduced amplification the signal goes into the overflow. The trigger cuts are used to disentangle the contributions.

The pure background (trigger request '$\overline{\text{SiPM1}}$ & $\overline{\text{SiPM2}}$') has entries up to 1000 QDC counts and shows an almost exponential decrease up to high QCD counts. The entries at high QDC counts are caused by very wide noise signals that have a high amount of charge in the signal but do not exceed the threshold. The signal of SiPM1 (in the SiPM1 spectrum) starts at about 100 QDC counts and has its maximum at ~ 500 QDC counts. The 'SiPM1 & SiPM2' signal is below this spectrum and shows none pronounced maximum. This difference between this spectrum and the spectrum of 'SiPM1' might be caused by inefficiencies of the SiPMs, e.g. a discriminator threshold that is too low and passes noise. So the events at the QDC counts 100-160 are most probably noise. Oppositional to the noise, the 'SiPM1 & SiPM2' events at low QDC counts are caused by very pronounced signals with a tight shape so that only a little amount of charge reaches the QDC.

The pure signal ('SiPM1 & SiPM2 & PMT') starts at ~ 400 QDC counts. The solid angle for muons that cause these spectra is confined as discussed in section 3.1. A most probable value (MPV) can be determined manually (MPV of SiPM1: ~1900, MPV of SiPM2: ~1600). Due to the same supply voltage requirements of the SiPMs this difference is most probably caused by the optical connection to the scintillator which varies because the SiPMs are placed manually. There are still signals that go into the QDC overflow in these cut spectra.

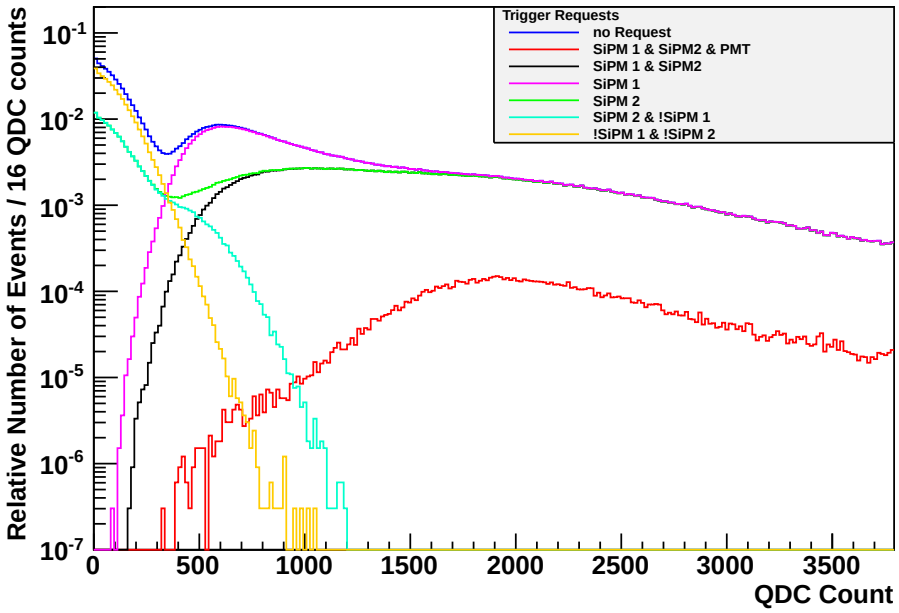

(a) Spectrum of SiPM1 of temperature-cleaned data

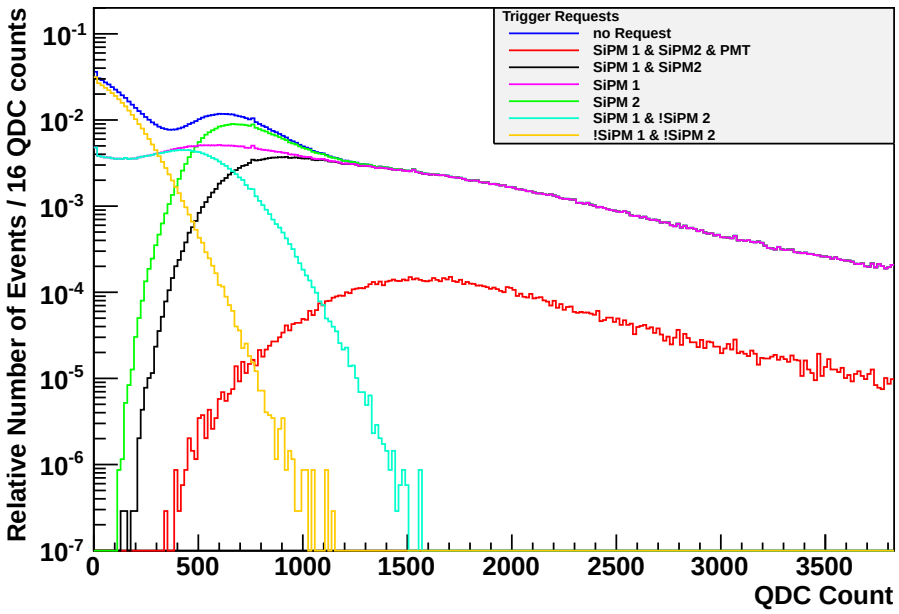

(b) Spectrum of SiPM2 of temperature-cleaned data

Figure 4.9: Spectra of the measurement with Tyvek (0.8 cm scintillator thickness)

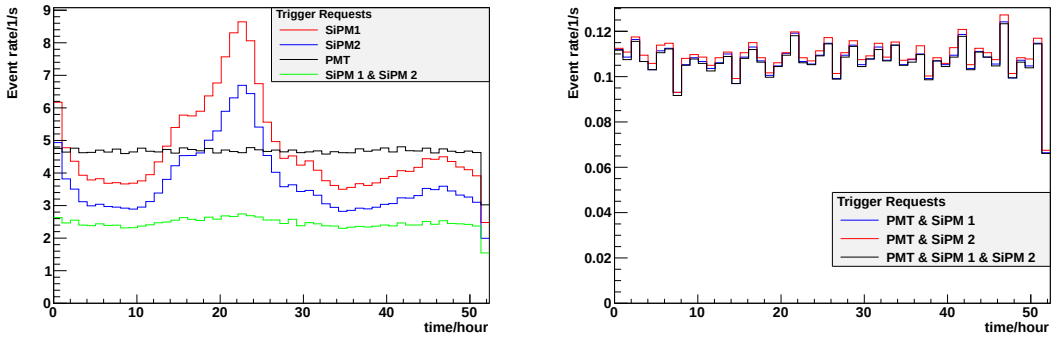

(a) Trigger rates for single detectors

(b) Trigger rates for vertical muons

Figure 4.10: Trigger rates of the measurement with Al-foil/bright side

Aluminium foil (bright side)

The trigger rates for this reflector behave similar to those for Tyvek (0.8 cm scintillator thickness). The rate for 'SiPM1 & SiPM2' (figure 4.10(a)) is at 2.4 $\frac{1}{s}$ which is little less than the same trigger rate for Tyvek but still in the area of 3.0 s^{-1}. The trigger rates shown in figure 4.10(b) are the same as in the Tyvek measurement. Therefore the detection efficiency for vertical muons did not change. That is also expected because the reflectivity is nearly the same (Al-foil (bright side): 88 %; Tyvek: 90 % (see table 4.3)).
The spectra (figures 4.11(a) and 4.11(b)) did slightly change. The MPV of SiPM2 (~ 1500) is almost the same compared to the Tyvek measurement while the MPV of SiPM1 is now ~ 1000 only. Due to that the spectra are temperature cut, a temperature change can not be responsible for this difference so that the varying optical connection of SiPM to the scintillator causes this MPV change. However noise and signal are well separated anyway.
The handling of the Al-foil turned out to be difficult, because it cracked at the scintillators edges when it was tightened to the scintillator. Therefore Al-foil is not a good candidate for a robust detector type.

Aluminium foil (dull side)

In difference to the previous measurements that were presented, the counting rate for the trigger request 'SiPM1 & SiPM2' (figure 4.12(a)) is at an average of 0.4 s^{-1}. Even the counting

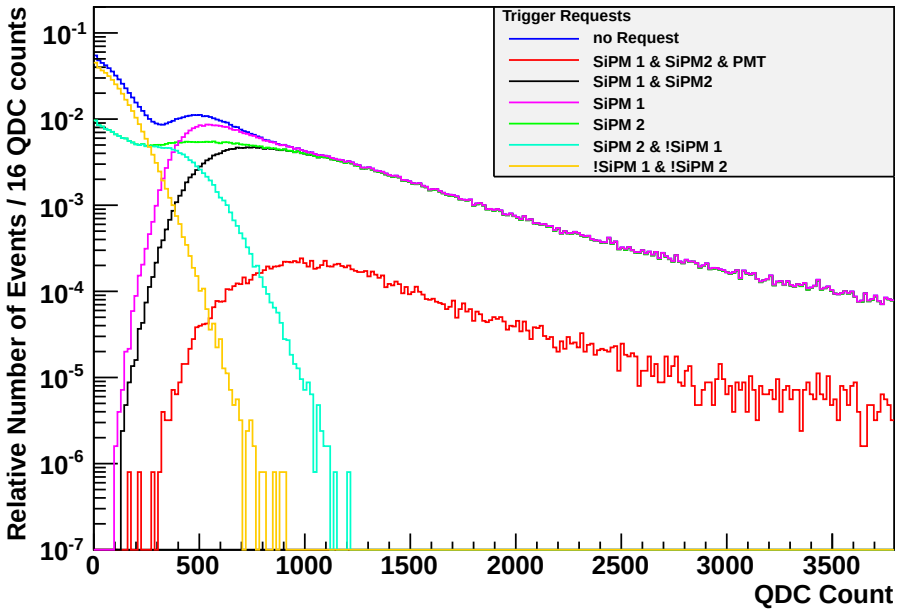

(a) Spectrum of SiPM 1 of temperature-cleaned data

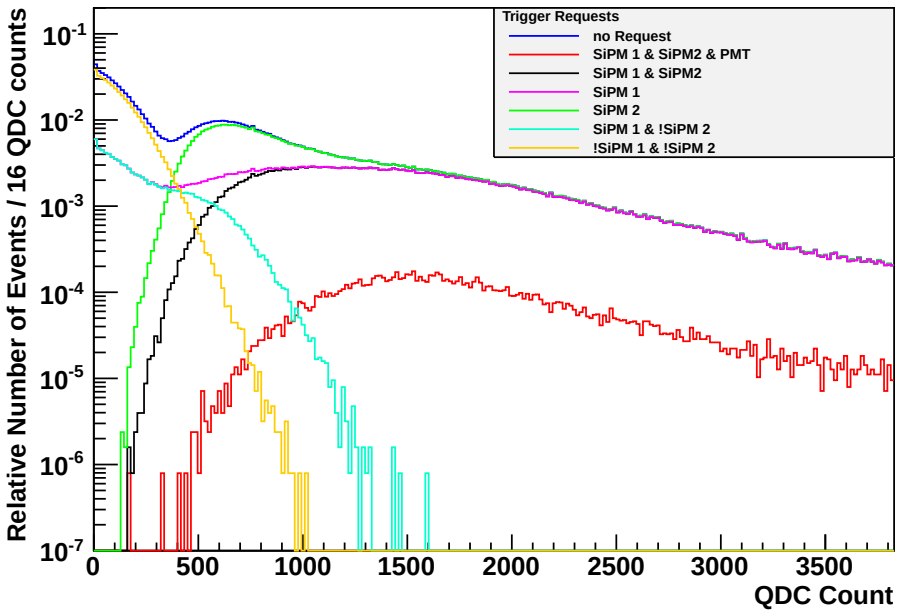

(b) Spectrum of SiPM 2 of temperature-cleaned data

Figure 4.11: Spectra of the measurement with Al-foil (bright side)

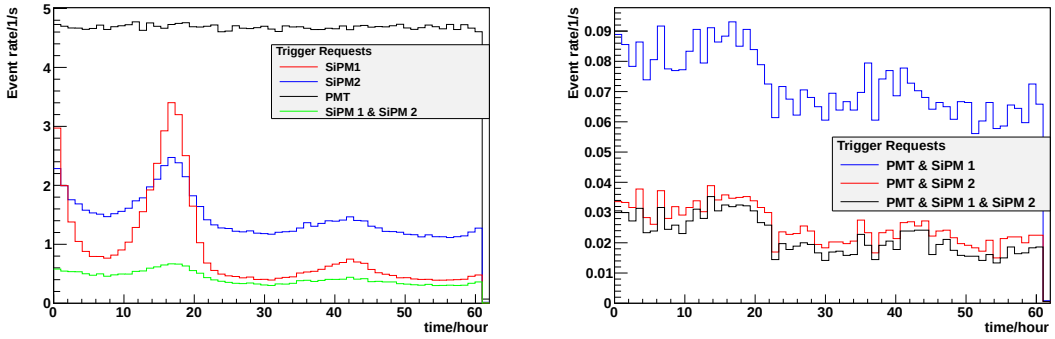

(a) Trigger rates for single detectors

(b) Trigger rates for vertical muons

Figure 4.12: Trigger rates of the measurement with Al-foil (dull side)

rates for the unique SiPM are always below the PMT counting rate. The SiPM signals seem to be too low to always fire a trigger signal when a muon hits the scintillator. The trigger rates in figure 4.12(b) are lower than 0.11 s^{-1}. This circumstance maintains the thesis that too few photons reach the SiPM.
The spectra (figures 4.13(a) and 4.13(b)) display a very low MPV (SiPM1: ~ 750; SiPM2: ~ 850) and the signal is not going into an overflow. An appropriate separation of signal and noise is not possible (see red and yellow line). Even the spectrum for 'SiPM1 & SiPM2' that includes almost horizontal muons creating much light due to the long path in the scintillator does almost not reach the overflow (especially SiPM2).

Black felt

The data of the measurement with no reflector is quite similar to the measurement with the dull side of the Al-foil. The counting rate for the 'SiPM1 & SiPM2' trigger request (figure 4.14(a)) is 0.6 s^{-1} - a little higher than the counting rate for the dull Al. One would even expect a lower rate because of the missing reflectivity, but the difference between felt and Al-foil (dull side) is so small that it blurs in the error caused by the optical connection and temperature.
The counting rates in figure 4.14(b) are different to each other. A difference in these counting rates seems to imply an insufficient type of detector (compare to the counting rates of mea-

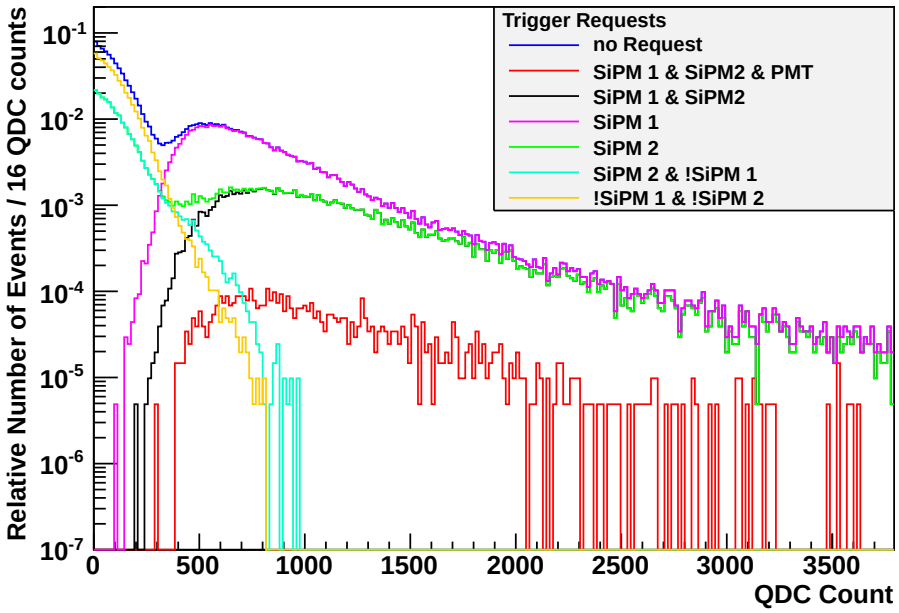

(a) Spectrum of SiPM 1 of temperature-cleaned data

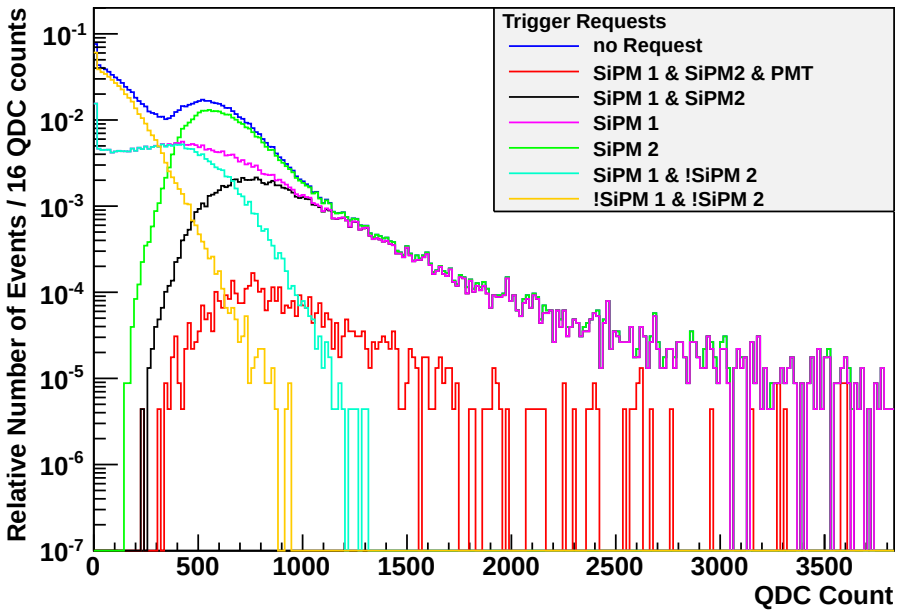

(b) Spectrum of SiPM 2 of temperature-cleaned data

Figure 4.13: Spectra of the measurement with Al-foil (dull side)

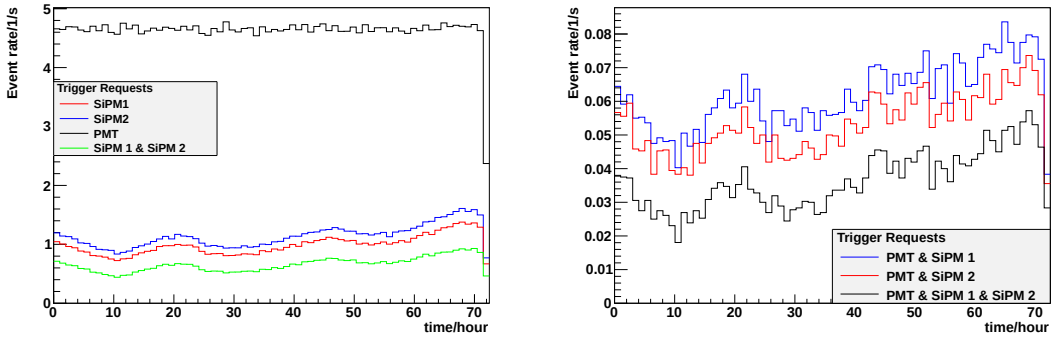

(a) Trigger rates for single detectors

(b) Trigger rates for vertical muons

Figure 4.14: Trigger rates of the measurement with black felt

surements with Al-foil (dull side) in figure 4.12(b)).
The spectra (figures 4.15(a) and 4.15(b)) show the same shape as the spectra of the dull Al with MPV of ~ 750 for SiPM1 and ~ 800 for SiPM2. The overlap of signal and noise is high again so that an appropriate separation is not possible in this case, too.

Tyvek (0.6 cm scintillator thickness)

The first thing to mention is that here the temperature was always higher than 28°C for this measurement (see table 4.4). Regardless of these high temperatures the event rates shown in figure 4.17(b) are at ~ 0.11 s^{-1} which corresponds to the other measurements with Tyvek and Al-foil (bright side) . The trigger rate for 'SiPM 1 & SiPM 2' (figure 4.17(a)) reaches 2.1 s^{-1}. So these trigger rates are much better than the trigger rates of the felt and the aluminium (dull side) measurements though the MPVs (figures 4.16(a) and 4.16(b)) are only about 800 (SiPM 1) and 1100 (SiPM 2). The scintillator has a thickness of 75% of the 0.8 cm thick scintillator. Therefore one would expect a MPV mean that is 75% of the MPV with the 0.8 cm scintillator but the MPVs are only 44 % (SiPM 1) and 70% (SiPM 2). The MPV of SiPM 2 would reproduce the prediction if the assumption is made that the optical connection of SiPM 2 is equal in both measurements. The missing 5% could be explained with the higher temperature. But the influence of temperature and optical connection on the MPV is not known separately so that this interpretation is daring and has to be verified in experiments with precisely controlled temperature and optical connection.

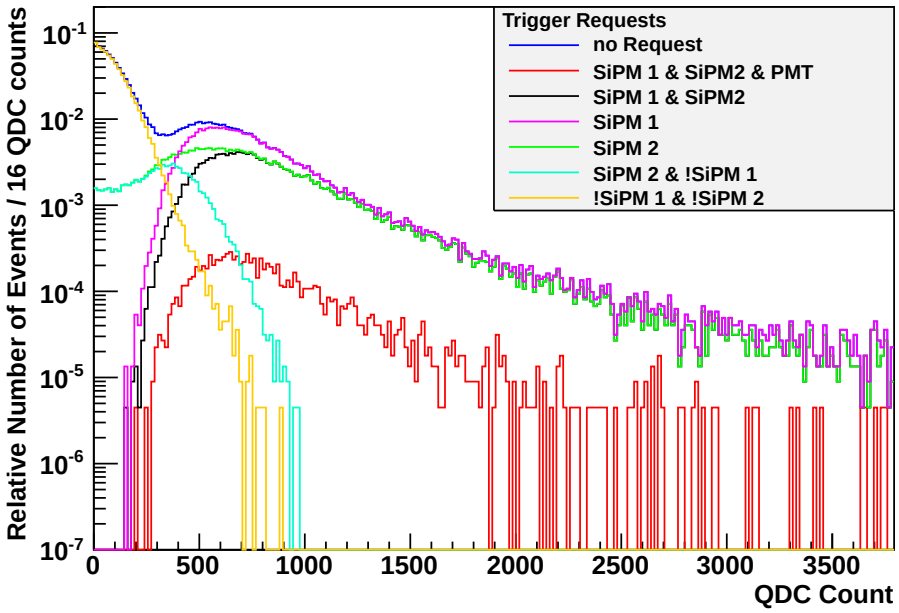

(a) Spectrum of SiPM 1 of temperature-cleaned data

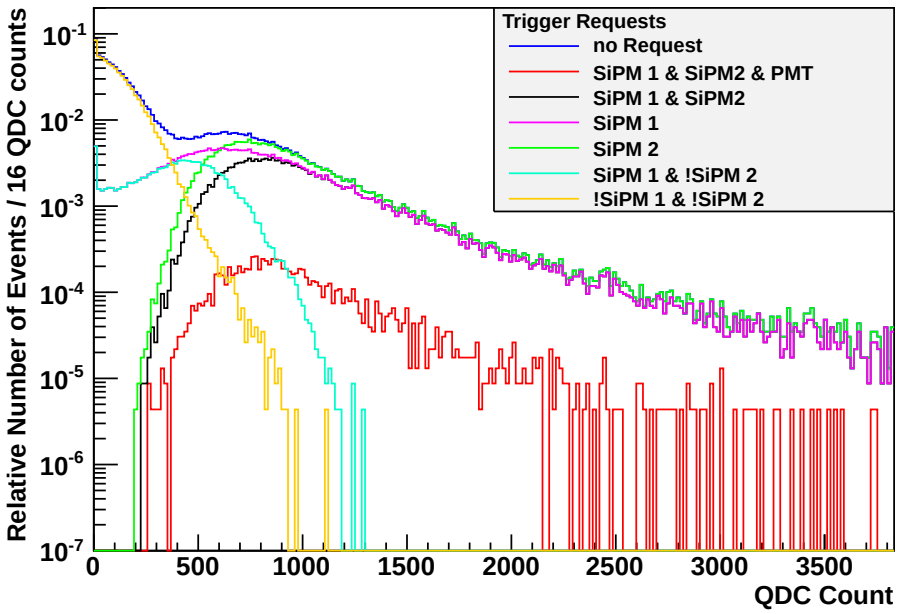

(b) Spectrum of SiPM 2 of temperature-cleaned data

Figure 4.15: Spectra of the measurement with felt

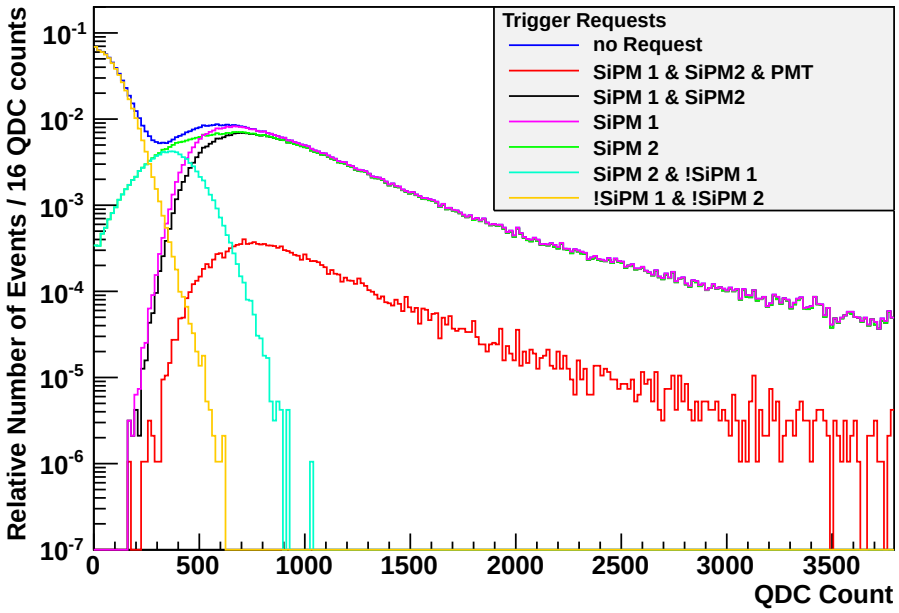

(a) Spectrum of SiPM 1 of temperature-cleaned data

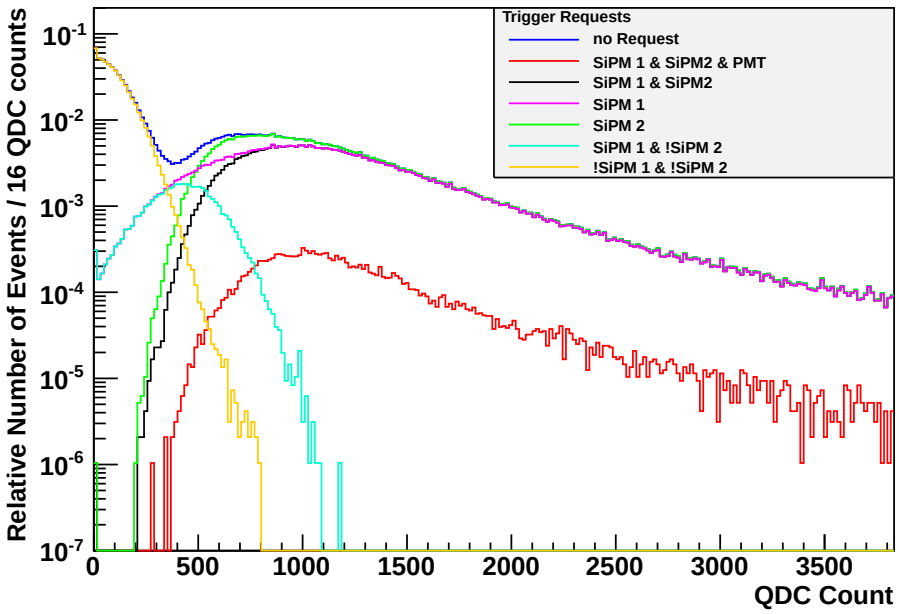

(b) Spectrum of SiPM 2 of temperature-cleaned data

Figure 4.16: Spectra of the measurement with Tyvek (0.6 cm)

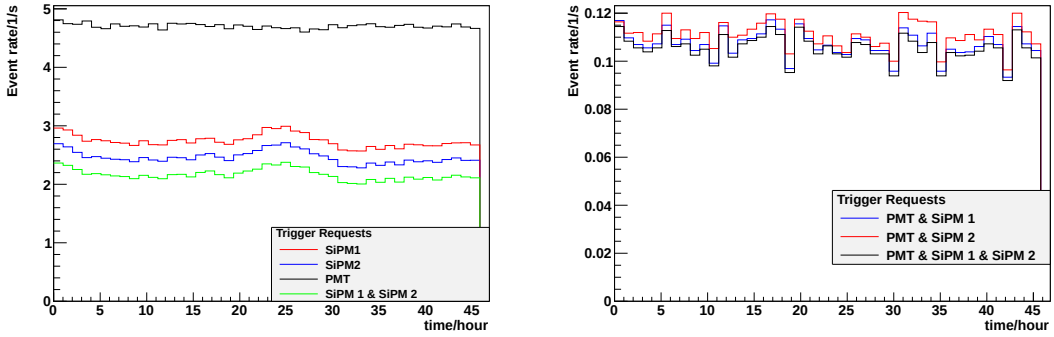

(a) Trigger rates for single detectors

(b) Trigger rates for vertical muons

Figure 4.17: Trigger rates of the measurement with Tyvek (0.6 cm)

4.2.5 Comparison

Measurement	Trigger rates (1/s)				QDC signal				QDC noise			
	PM	S1	S2	S1&S2	S1	<RMS>	S2	<RMS>	S1	<RMS>	S2	<RMS>
Tyvek(0.8)	4.5	6.3	5.7	3.0	2227	614	1896	643	106	89	132	111
Tyvek(0.6)	4.5	2.6	2.4	2.1	1008	479	1280	553	84	66	101	81
Al(bright)	4.6	4.7	3.7	2.4	1321	591	1851	652	104	86	128	107
Al(dull)	4.5	0.9	1.4	0.4	1079	544	915	425	91	78	109	94
felt	4.6	1.0	1.1	0.7	841	432	1002	460	89	74	110	95

Table 4.5: Average data of the measurements

A list of average data is shown in table 4.5. The RMS is a quantity for the width of the spectrum.

The measurements can hardly be compared quantitatively because of the unknown and/or uncontrollable parameters temperature and optical connection of the SiPM. A difference between good and bad reflectors can be observed. A good reflector around the scintillator improves the light yield that signal and noise are well divided. A scintillator with 0.6 cm thickness might also create enough light to clearly seperate signal and noise, but this has to be determined in later tests. Both measurements with Tyvek indicate that the QDC count and thus the light yield in the scintillator go linear with its thickness as it is expected.

The aluminium foil is an improper reflector because of its instability in the handling though the reflectivity of the bright side would be sufficient. Because of the qualitative measure-

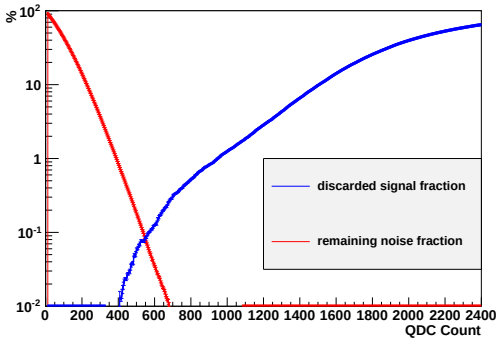

(a) Tyvek (0.8 cm), SiPM 1

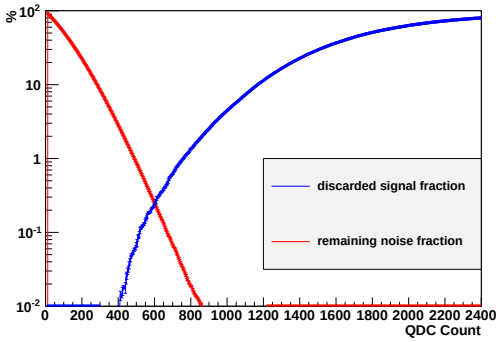

(b) Tyvek (0.8 cm), SiPM 2

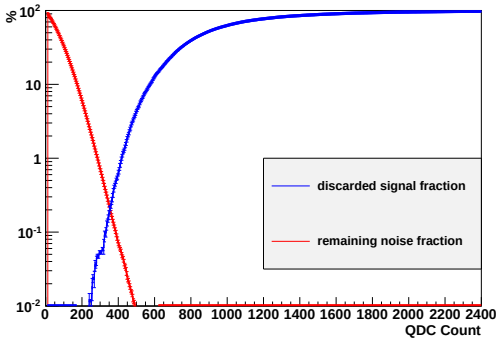

(c) Tyvek (0.6 cm), SiPM 1

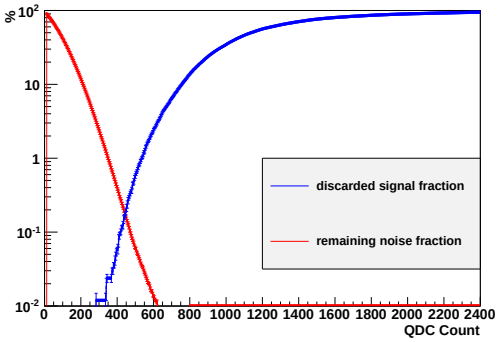

(d) Tyvek (0.6 cm), SiPM 2

Figure 4.18: Percentage of signal and noise for QDC thresholds for both SiPMs

ments Tyvek is the recommended reflector. It is tear- and waterproof, has a good reflectivity of 90% and is comparatively inexpensive that huge areas can be covered with Tyvek as it is already done at the Pierre Auger Observatory in Argentina [24] and the Super Kamiokande in Japan [25].

Introducing the quantities noise fraction

$$f_{\text{noise}}(x) = \frac{\int_{Q \leq x} n(Q)\, dQ}{\int n(Q)\, dQ} \tag{4.1}$$

and signal fraction

$$f_{\text{signal}}(x) = \frac{\int_{Q>x} s(Q)\, dQ}{\int s(Q)\, dQ} \tag{4.2}$$

it becomes obvious that a cut on the QDC count or digitalized charge can separate signal from noise. Plotting the noise and signal fractions depending on a QDC threshold (figure 4.18) shows that a threshold of 400 counts for the Tyvek (0.8 cm scintillator thickness) measurement and of approximately 250 counts for the 0.6 cm thick scintillator separates the full signal with 1-3% noise left. If both measurements would have been taken at the same temperature, the curvature for the left noise should be the same. Because of the high temperatures in the measurement with the 0.6 cm thick scintillator the data shifts to lower counts.

5 Comparison of measurement and simulation

5.1 Detector simulation with GEANT4

The data discussed in the following was generated with the simulation program GEANT4. For this purpose the geometry of the setup and the physical characteristic of the scintillator have been modeled accurately. The exact simulation setup is described in Andreas Künskens bachelor thesis [4]. The simulated data is also taken from this thesis.
The (10 x 10 x 0.8) cm^3 and the (10 x 10 x 0.6) cm^3 BC-404 scintillators (the same scintillator as in the measurement (see also 3.1.1)) have been simulated with reflections of 98%, 95%, 80% (diffuse and specular reflector) and without reflectors. Two SiPMs are placed on the scintillator with attributes identical to the S10362-33-100C (see 3.1.2). The scintillator was simulated with a surface roughness between 0° and 5° which is a quantity for how good the scintillator yields total reflectivity (0° = absolute flat surface). For the comparison the roughness between 2° and 4° is evaluated, because the scintillator is not completely flat even if it is diamond polished.
Vertical muons are detected with the scintillator and the number of photons that hit the SiPM is counted. Every Pixel of the SiPM can only be hit once, because one expects that the event is over till the pixel is ready again. So photons that hit one pixel that already has been hit in the event are not counted.
A landau-fit was applied to the data to determine the most probable value (MPV) for the number of photons that hit the SiPM. The full results are shown in figures 5.1(a) and 5.1(b).
It is obvious that it does not matter, if the reflector is diffuse or specular. A list of the photon detection counts for the simulations that are relevant for the comparison is given in table 5.1. The number of photons is given in the range 2° - 4° surface roughness.

Scintillator thickness	Reflectivity	Number of photons
8 mm	98%	70-90
8 mm	95%	38-50
8 mm	80%	11-14
8 mm	0 %	4-7
6 mm	95 %	31-36

Table 5.1: Results of the simulations [4]

5.2 Comparison

For the comparison it is assumed that the QDC count is proportional to the number of photons that hit the SiPM because the SiPM is operated in the Geiger mode and will release the almost the same charge at every pixel that is hit.
The list of the MPVs in the measured data is given in table 5.2. The results for measurement and simulation are plotted in figure 5.2. The results for black felt and the dull side of the Al-foil are consistent with the simulations if an offset of ~600 QDC counts is subtracted. Too few photons reached the SiPM so that the MPV is dominated by noise signals which are due to the rather high temperatures. These signals provide an MPV that is consequently almost the same for both measurements. Therefore the subtraction is reasonable.
The other measurements had mainly signals that were provided by real muon detection. For that reason, the QDC count can not be shifted by the 600 QDC counts, too. But the measurements and the simulations show that a reflector has to have a reflectivity higher than 80 % to make a measurable contribution to the light yield. Due to the fact that the setup with the bright side of the aluminium foil and Tyvek as reflectors have almost the same reflectivity, one expects the same MPV for the number of photons that hit the SiPM. This was discussed in 4.2.4. Because of the missing conversion factor between QDC count and number of photons a further comparison with the simulated data is impossible. The fact that the simulated MPV is the same for two simulations with the same reflectivity is trivial.
A last comparison between simulated and measured data has to be done with the measurements of Tyvek (0.8 cm) and Tyvek (0.6 cm). Interestingly the Tyvek (0.6 cm) simulation expects not exactly an MPV that is 75% of the MPV of the 0.8 cm Tyvek simulation but an MPV of 72% - 81%. This is an effect in the simulation that is referred to the geometry of the scintillator, because further evaluations show that the number of emitted photons in the 0.6 cm

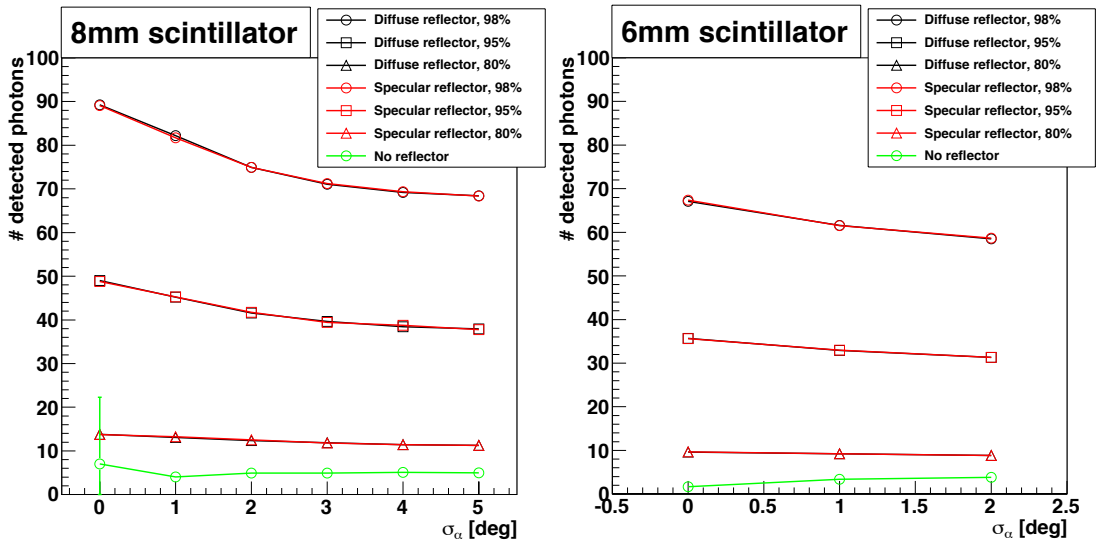

(a) Simulation result for the (10 x 10 x 0.8) cm^3 scintillator

(b) Simulation result for the (10 x 10 x 0.6) cm^3 scintillator

Figure 5.1: Simulation results [4]

scintillator is exactly 75% of the number of the 0.8 cm scintillator, as it is expected. For further information see [4].

The measurements are too imprecise to check this prediction. The data shows at least for SiPM 2 that the MPV of the measurement with the 0.6 cm thick scintillator is ~ 70% of the MPV of the measurement with the 0.8 cm thick scintillator, which agrees with the simulation. The reasons for the discrepancy at SiPM 1 was discussed in section 4.2.4.

All in all the simulation fits to the measurements when the huge errors in the measurement caused by the temperature change and the varying optical connection in the different measurements are considered.

Scintillator thickness	Reflectivity	MPV of QDC count (SiPM 1)	(SiPM 2)
8 mm	90% (Tyvek)	1900	1600
8 mm	88% (Al-foil(bright side))	1000	1500
8 mm	80% (Al-foil(dull side))	750	850
8 mm	0 % (Black felt)	700	850
6 mm	90 % (Tyvek)	750	1100

Table 5.2: Results of the measurements

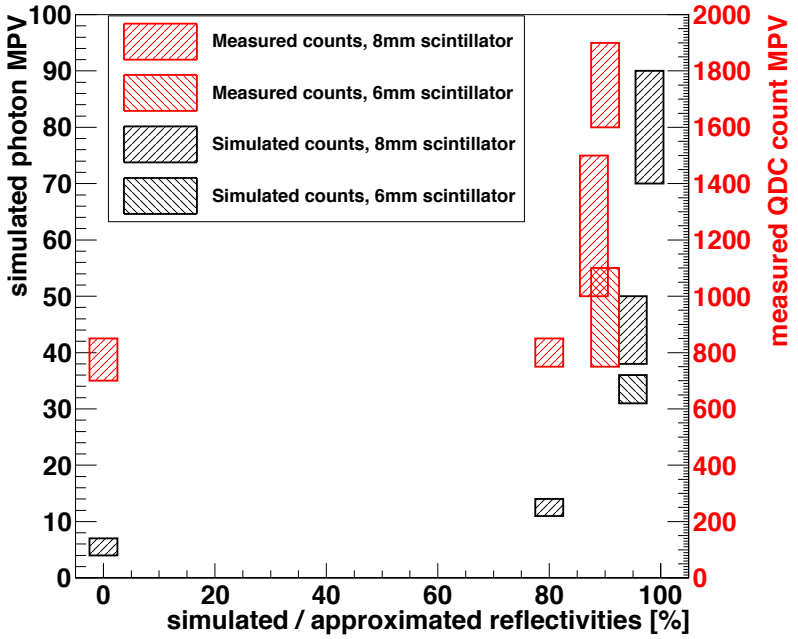

Figure 5.2: Correlation of measured QDC Counts and simulated photon MPVs

6 Conclusion & Outlook

The measurements showed that it is possible to measure cosmic muons with the detector prototype. The SiPM signals are high enough to separate noise from signal. Measurements and counting of cosmic muons have been provided. Therefore the full setup with power supply for SiPMs and amplifier boards and the processing of the gained signals, including its discrimination, has been established. The onboard temperature sensors and sensors inside the blackbox have been put into operation. The amplifier boards were measured, too.
Though the measurements of cosmic muons did not yield quantitatively comparable data, many problems were identified what will help to improve the detector prototype. The biggest problem is the temperature dependency of the SiPMs. For appropriate measurements the supply voltage has to be permanently adjusted dependent to the temperature. Another solution would be a temperature control at the SiPM. Is has to be checked which alternative occupies a smaller volume and is more accurate and manageable.
A next step can be the check, whether the amplifier boards are necessary. The gain of the integrating output is about 2 for low frequencies (consider that the measurements of the amplifier boards have been performed with an old amplifier version (see section 4.1.1)). It might be possible to see the SiPM signals even without a pre amplification. If this is possible, the volume that is occupied by the detector would be much smaller and almost only defined by the scintillator. Such tests will be progressed in the near future by Maurice Stephan.
If the amplifier is still necessary, the board has to be improved to reduce the resonances and reach a constant gain over the whole frequency range at best.
Dedicated tests with the prototype are needed to get the efficiency and evaluate a photon equivalent for the QDC counts.
Also larger scintillators can be tested to see, if enough light reaches the SiPMs, to see a signal when the module has e.g. a size of (25 x 25 x 0.8) cm^3.
When the temperature problem and the problem with the optical connection are solved, noise and signal might be so well distinguishable that one SiPM per scintillator only is sufficient to detect muons. This has to be checked.
So the measurements detected some problems but also a good reflector candidate has been

found. Tyvek is an inexpensive and easy manageable reflector with a good reflectivity that is sufficient for the scintillators reflector.
All in all the measurements showed that the direct readout is a considerable alternative for muon detectors with much potential.

7 Appendix

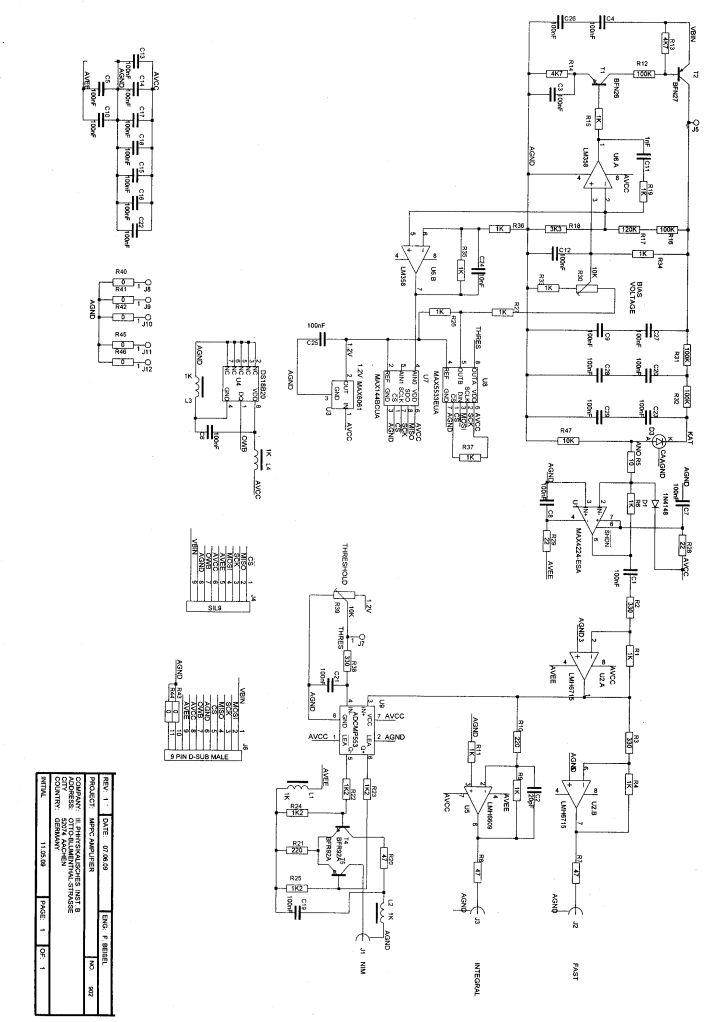

Figure 7.1: Circuit diagram of the SiPM frontend boards [F. Beißel, private communication]

Bibliography

[1] *Calorimeters for the SLHC and VLHC*, October 2003.

[2] *Photomultiplier Tubes, Basics and Applications*. Hamamatsu Photonics K. K., 3 edition, 2006.

[3] November 2009. URL `http://lmu.web.psi.ch/facilities/electronics/TDC/CFD_signals.png`.

[4] Andreas Künsken. *Simulation of a detector prototype with direct SiPM-readout and comparison with measured data*. Bachelor thesis at the RWTH Aachen University, August 2010.

[5] C.A.E.N. *Mod. V965/V965A 16/8 Ch. Dual Range QDC*, July 2008.

[6] CMS Collaboration. *The CMS experiment at the CERN LHC*. IOPscience, August 2008.

[7] Wolfgang Demtröder. *Experimantalphysik 4*. Springer-Verlag, Berlin Heidelberg New York, Erwin-Schrödinger-Strasse 46, 67663 Kaiserslautern, 3 edition, 2009.

[8] DETEC. Scintillating products. Presentation, 2006.

[9] EA - Elektro-Automatik, D-41747 Viersen, Helmholtzstr. 31-37. *Labornetzgerät/Laboratory Power Supply EA-PS 2316-050*.

[10] Elektro-Automatik. *EA-PSI 6000, Programmierbare Labornetzgeräte*.

[11] T.K. Gaisser and T. Stanev. Cosmic rays. 2007.

[12] Particle Data Group. Particle physics booklet, 2008.

[13] Hamamatsu Photonics K.K., Japan. *MPPC (multi-pixel photon Counter, S10362-33 series, S10931 series)*, 2009.

[14] Joseph F. Hanlon. *Handbook of Package Engineering*. PA and Technomic Publishing, 1992.

[15] A. Zepeda J.C. Arteaga-Velazquez, C. Vazquez-Lopez. A measurement of the diffuse reflectivity of 1056 tyvek in air and water. Technical report, Department of Physics, CINVESTAV-IPN, Mexico, Distrito Federal, Apartado Postal 14-740, 07000 Mexico, 2005.

[16] Jörg Rennefeld. *Studien zur Eignung von Silizium Photomultipliern für den Einsatz im erweiterten CMS Detektor am SLHC*. Diploma thesis at the RWTH Aachen University, February 2010.

[17] LeCroy Corporation. *WaveJet 300 Series Oscilloscopes*, 2006.

[18] Dr. Gerhard Lutz. *Semiconductor Radiation Detectors*. Springer-Verlag, Berlin Heidelberg New York, 2007.

[19] Maxim Integrated Products, 120 San Gabriel Drive, Sunnyvale, CA 94086. *DS18B20 Programmable Resoltion 1-Wire Digital Thermometer*, 2008.

[20] Dr. Oliver Pooth. Teilchendetektoren, 2010.

[21] Curt A. Moyer Raymond A. Serway, Clement J. Moses. *Modern Physics*. Thomson Learning, Inc., Brooks/Cole — Thomson Learning, 10 Davis Drive. Belmont, CA 94002, USA, 3 edition, 2005.

[22] D. Renkera and E. Lorenz. Advances in solid state photon detectors. *IOPscience*, 2009.

[23] Saint-Gobain Crystals, Hiram, OH 44234, 17900 Great Lakes Parkway. *BC-400, BC-404, BC-408, BC-412, BC-416, Premium Plastic Scintillators*.

[24] University of Mississippi. *Measurements of TYVEK Reflective Properties for the Pierre Auger Project*. Justus Ogwoka Gichaba, August 1998.

[25] XXIV International Cosmic Ray Conference. *Contributions from the SuperKamiokande Collaboration*. Rome, Italy, September 1995.

Acknowlegdements

Mein erster Dank gilt Herrn Prof. Hebbeker, der mir überhaupt erst die Möglichkeit geboten hat, eine Bachelorarbeit an seinem Institut zu verfassen und Forschungs- und Büroplätze zur Verfügung gestellt hat.
Großer Dank gebührt auch Markus Merschmeyer und Paul Papacz, die beide mit ihrem unermüdlichen Einsatz diese Bachelorarbeit ermöglicht haben. Ohne diese Hilfen und anregenden Diskussionen wäre ich heute nicht da, wo ich stehe. Diese Arbeitsumgebung hat erst den Grundstein zu solchen Fortschritten (sowohl in der Bachelorarbeit, als auch persönlich) gelegt.
Daher geht mein Dank auch an das gesamte Institut IIIA, in dem ich vom ersten Tag an herzlich aufgenommen wurde und mich direkt als vollwertiges Institutsmitglied verstanden fühlte. Dies schließt auch die Verwaltung und unsere Sekretärin Adriana del Piero ein.
Die Arbeit der Mechanik- und Elektronikwerkstatt war ebenfalls essentiell für den Fortschritt dieser Arbeit. Herzlichen Dank an alle dortigen Mitarbeiter.
Da eine Bachelorarbeit auch immer Unterstützung aus dem privaten Umfeld bedarf, geht ein besonderer Dank an meine Eltern, die es mir ermöglicht haben mein Physikstudium aufzunehmen und mich ständig unterstützen. Auch wenn sie ab und an verzweifeln, wenn ich wieder physikalische Phänomene erkläre und kein Wort verstanden wird, haben sie doch immer Geduld mit mir und unterstützen meine Arbeit.
Ein weiterer Dank geht an meine Freundin Ina, die in der letzten Zeit viel auf mich verzichten musste und mich doch immer wissen lässt, dass sie für mich da ist.
Zu guter letzt danke ich allen, die mir in irgendeiner Art und Weise Unterstützung und Inspiration für diese Arbeit waren und nicht erwähnt wurden. Es ist nicht möglich all diese aufzulisten, doch soll ihnen mein Dank gewiss sein.

Erklärung

Ich versichere, diese Arbeit selbstständig verfasst und keine anderen als die angegebenen Hilfsmittel und Quellen benutzt zu haben.
Aachen, 03. August 2010

Florian Scheuch